Environmental Technology & Innovation 25 (2022) 102148

Contents lists available at ScienceDirect

Environmental Technology & Innovation

journal homepage: www.elsevier.com/locate/eti

Thermodynamics, isotherms, and mechanisms studies of lithium recovery from seawater desalination reverse osmosis brine using roasted and ferrocyanide modified date pits

Rana S. Al-Absi [a], Mohammed H. Abu-Dieyeh [b], Radhouane Ben-Hamadou [a], Mustafa S. Nasser [c], Mohammad A. Al-Ghouti [a,*]

[a] Environmental Science program, Department of Biological and Environmental Sciences, College of Arts and Sciences, Qatar University, State of Qatar – Doha. P.O. Box: 2713
[b] Biological Sciences program, Department of Biological and Environmental Sciences, College of Arts and Sciences, Qatar University, State of Qatar – Doha. P.O. Box: 2713
[c] Gas Processing Center, College of Engineering, Qatar University, Doha, State of Qatar, Qatar

ARTICLE INFO

Article history:
Received 31 August 2021
Received in revised form 18 November 2021
Accepted 18 November 2021
Available online 3 December 2021

Keywords:
Agricultural waste
Valuable metals
Brine
Thermodynamics
Adsorbent modification

ABSTRACT

In this study, the adsorption isotherms and thermodynamic studies of lithium ions from seawater reverse osmosis (SWRO) desalination brine were investigated. Three adsorbents were utilized namely, roasted date pits (RDP), potassium copper, and nickel hexacyanoferrate-date pits (RDP-FC-Cu and RDP-FC-Ni). The prepared adsorbents showed enhanced morphological and chemical structures such as high porosity, carbonaceous composition, larger pore and volume sizes, smaller particle sizes as well as the presence of unique functional groups on their surface. The adsorption of lithium ions onto the three adsorbents was enhanced with an increase in solution temperature and initial lithium concentration. The temperature that showed the highest adsorption of lithium ions onto the three adsorbents was 45 °C. The adsorption of lithium ions onto the three adsorbents was the highest at an initial lithium concentration of 100 mg/L. The three adsorbents achieved an adsorption capacity of around 99 mg/g at the optimum temperature and initial concentration. On the other hand, RDP-FC-Cu achieved the highest adsorption capacities for lithium ions at all the studied initial concentrations. The thermodynamic study showed that the adsorption process of lithium ions onto the adsorbents is endothermic, spontaneous, and favorable at all the studied temperatures (25 °C, 35 °C, and 45 °C). Moreover, the adsorption of lithium ions onto the three adsorbents followed the Langmuir, Freundlich, Dubinin–Radushkevich, and Temkin adsorption isotherm models differently at each studied temperature. For RDP, the adsorption process followed the Freundlich adsorption isotherm model at 25 °C, while it was more fitted to the Langmuir isotherm model at 45 °C and all models at 35 °C. The adsorption of lithium ions onto RDP-FC-Cu followed Langmuir adsorption isotherm model at 25 °C and 35 °C, while it fitted all models at 45 °C. On the other hand, Langmuir and Dubinin–Radushkevich isotherm models were best fit for the adsorption of lithium ions onto RDP-FC-Ni at 25 °C and 35 °C. The desorption study presented 99% desorption percentages of lithium ions from all the adsorbents, which showed the great regeneration potential of the adsorbents. Furthermore, the selectivity study showed that RDP-FC-Cu achieved 99.9% adsorption removal of lithium ions from the SWRO brine

* Corresponding author.
E-mail address: mohammad.alghouti@qu.edu.qa (M.A. Al-Ghouti).

https://doi.org/10.1016/j.eti.2021.102148

while RDP-FC-Ni and RDP achieved 99.8% and 99.3% adsorption removals, respectively. Finally, the cost analysis revealed that the total cost for the preparation of the adsorbent was 29.81 USD.

1. Introduction

The quantity and quality of the world's water resources are impacted by human and natural factors, which are often interlinked. The continuous increase in populations, urbanizations, and industrialization are some of the leading human factors that largely affect water resources (Mvulirwenande and Wehn, 2020). Population growth is accompanied by industrialization and economic growths and all together pose pressures on the water demands around the world. In addition, industrial activities are well-known contributors to air, land, and water pollution. This is because industries usually involve environmental discharges, the use of chemicals, and water requirements (Wan and Wang, 2021). On the other hand, the natural factors that impact the world's water resources availability include climatic conditions, the hydrological cycle, natural disasters as well as resource distributions (Habiyaremye, 2020). For example, semi-arid and arid countries like the Gulf Council Countries (GCC) are often characterized by low rainfall, extreme weather conditions including long summers as well as a shortage in natural water resources (Mannan et al., 2019). Countries with high rainfall, lakes, and rivers do not usually experience the same water shortages as the GCC. The GCC countries are surrounded by sea, which provides their growing populations with a water resource (Rahman and Zaidi, 2018). Countries that rely on seawater for their national domestic water requirements face the challenge of producing freshwater from saline seawater. Seawater desalination is a worldwide well-established method that provides freshwater from seawater. Employing seawater desalination to produce potable water requires major technological investments as well as research and training. Therefore, in the Gulf region where the economic status and aridity of countries are relatively high, the implantation of seawater desalination is successful (Nassrullah et al., 2020). It was recently estimated that the GCC countries produce more than 50% of the world's desalinated water (Ibrahim and Eltahir, 2019). To be more specific, Qatar is characterized by high population and economic growth as well as high overall standards of living. These characteristics caused the country to have one of the highest water per capita consumption rates in the world. The increase in populations and water consumption rates are the main drivers for the high reliance on desalination technology (Mannan et al., 2019). In addition, the great economic stability of Qatar due to the fossil fuel industry provided the country with one of the largest capacities for desalination around the world. 99% of the municipal accessible water in Qatar is accounted for by the desalination industry. On the other hand, groundwater resources provide Qatar with only 1% of its freshwater requirements. Freshwater produced from seawater desalination in Qatar is in continuous increase where it was estimated to be around 493 million metric cubes in 2014 and 540 metric cubes in 2017 (Rahman and Zaidi, 2018; Baalousha and Ouda, 2017).

Seawater desalination could be accomplished by various technologies. There are two main categories for seawater desalination technologies and those are thermal and membrane-based desalination (Al-Absi et al., 2021a,b). Membrane-based desalination technologies, especially reverse osmosis (RO), are gaining the world's interest in desalinating seawaters. This is because of its significantly lower energy consumption requirements and implementation costs coupled with its high freshwater production capacity (Kim et al., 2019). The implementation of seawater desalination can be coupled with various challenges and impacts. Some of these challenges are related to infrastructure, labor, and construction investments. In addition, the production of freshwater from seawater through desalination requires the addition of various pre-treatment chemicals such as additives, coagulants, flocculants, and biocides. The leakage of such chemicals to the environment or the produced freshwater could pose deleterious negative marine and health impacts (Darwish et al., 2013; Lee and Jepson, 2021). A seawater desalination by-product known as brine is a major challenge due to its characteristics. Brines produced from the desalting of seawater are often characterized by high salinities, temperatures, total dissolved solids as well as metals. Also, brines usually have altered pH ranges and contain various kinds of pre-treatment chemicals. These characteristics make seawater desalination brines extremely dangerous for the health of marine organisms as well as human health (Elsaid et al., 2020). Therefore, there is a global need for effective management of desalination brines and specifically the remediation of their toxic nature (Kim and Min, 2020). Seawater desalination brines often contain various kinds of metal ions which could be useful for many industrial applications (Wang et al., 2019). For example, lithium is a commercially and industrially valuable metal that is used in the manufacturing of batteries, ceramics, polymers, greases, and additives (Gaztañaga et al., 2020). The method of adsorption could be a potential solution for the remediation and recovery of metal ions from RO desalination brine streams.

Adsorption is a mass transfer process that is efficient, economic, simple, and selective towards specific pollutants and is widely applied for the removal of many targeted substances from seawaters, wastewaters, and brine streams (Tang et al., 2021). The adsorption technique is based on the adherence of pollutants (Adsorbates) onto the surface of a material, called the adsorbent. Some of the factors that influence adsorption processes' effectiveness include solution pH, the adsorbate's concentration, the presence of competing ions, adsorbent dosage, and temperature. The temperature at

which adsorption systems are employed largely contributes to the overall adsorption capacities, efficiencies, and behaviors (Yang et al., 2019). Many important adsorption parameters like entropy, enthalpy, and Gibbs free energy are defined by thermodynamics. These parameters help scientists in defining adsorption systems as spontaneous, favorable, endothermic, or exothermic (Yadav et al., 2021). Thermodynamics provides significant insights regarding the adsorption tendencies, behaviors, and energy requirements as well as cost and overall sustainability (Al-Ghouti and Al-Absi, 2020).

Palm trees are native plants in the GCC countries like Qatar and the palm tree industry produces massive amounts of dates annually. Along with the production of dates, great quantities of date pits are produced as wastes. Date pits could serve as effective adsorbents or support materials for other adsorbents for the adsorption of metal ions. This is due to their high adsorptive characteristics and great abundance (Al-Ghouti et al., 2019). Combining the great adsorptive potentials of date pits with other effective adsorbents would lead to the production of extremely effective and cost-friendly adsorbents. For example, metal hexacyanoferrates are known as coordination polymers that have special cubic lattice structures that support the adsorption of pollutants. These polymers contain a transition metal ion such as Fe^{3+}, Cu^{2+}, Ni^{2+} and Co^{2+} and C≡N coordinated bridges (Oliveira et al., 2018). The mechanism of adsorption between a metal hexacyanoferrate and pollutant-like metal ions involves an ion exchange between the pollutant and the transition metal (Wang et al., 2018). Their high selectivity towards a variety of pollutants and insolubility makes metal hexacyanoferrates excellent adsorbents for metal extraction and recovery. In addition, the synthesis processes of metal hexacyanoferrates are simple and cost-effective that involves a precipitation reaction between transition metals and the precursors (Kim et al., 2017a,b). Due to their submicron size, the effective application of metal hexacyanoferrates requires the usage of support materials with adsorptive capabilities. This study involves the investigation of the adsorptive efficiencies of roasted date pits as towards lithium ions from RO seawater desalination brines in Qatar. In addition, this study focuses on exploring the influence of temperature and thermodynamics on the recovery process of lithium ions. Moreover, many adsorption isotherm models aim at describing the mechanism of adsorption between the adsorbent and the adsorbates. The adsorption isotherm models can achieve an understanding of the quantity of adsorbed and non-adsorbed adsorbate molecules as well as the distributions of the adsorbate molecules at different equilibrium temperatures and concentrations (Can et al., 2016). The adsorption isotherms take into account the influence of temperature on the adsorption capacity (qe) of the adsorbent. Several models have been developed with the most studied ones being Langmuir, Freundlich, Dubinin–Radushkevich, and Temkin isotherm models (Núñez-Gómez et al., 2019).

In this study, roasted date pits (RDP) were used as support materials for potassium hexacyanoferrates to synthesize effective and novel composite adsorbents from natural agricultural wastes. The roasted date pits composite materials were potassium copper hexacyanoferrate-date pits (RDP-FC-Cu) and potassium nickel hexacyanoferrate-date pits (RDP-FC-Ni). These composite materials were synthesized to mainly examine their selectivity as well as adsorptive capabilities towards lithium ions in comparison with unmodified roasted date pits. The physiochemical characteristics of the three adsorbents were examined using a variety of analytical techniques. The adsorption experiments were performed under a variety of temperatures and the adsorption thermodynamics, as well as isotherms, are presented. To establish a complete understanding of the adsorbent–adsorbate interactions under the influence of temperature and their characteristics, a detailed overview of the adsorption mechanisms is presented. Finally, the cost-effectiveness of synthesizing the roasted date pits and the novel composite materials are analyzed to test the real applicability of this study. The novelty of this study is that it combines the high adsorptive capabilities of roasted date pits with two metal hexacyanoferrate-based adsorbents to recover the highly valuable lithium ions from Qatari-based RO desalination brine. In addition, Qatar is one of the leading countries in the production of RO desalination brines and date pits as two major wastes. Therefore, utilizing date pits to treat RO brines would serve a great environmental and economical benefit to the country.

2. Materials and methods

2.1. Collection, preparation, and physiochemical characterization of the adsorbents

Previous work done by Al-Absi et al. (2021a,b) involved the collection, preparation, and physiochemical characterization of the date pits adsorbent. To obtain a full understanding of the following adsorption and desorption experiments, a summary of the work is presented in this study. The methodology of the adsorbent's preparation involved removing impurities and moisture by washing the date pits with distilled water then drying them for 24 h. at 100 °C. The date pits were roasted at 100 °C for 6 mins on a hot plate with continuous mixing until they obtained a golden color. After roasting, the roasted date pits (RDP) were sieved to form different particle sizes (100–250 μm, 250–500 μm, and 500–750 μm). The RDP was then used as supporting materials for the ferrocyanide-date pits modifications. Ultimately, two other adsorbents were generated as potassium copper and nickel hexacyanoferrates denoted as RDP-FC-Cu and RDP-FC-Ni, respectively. In short, the synthesis of the RDP-FC-Cu and RDP-FC-Ni consisted of three main steps. Firstly, a 1:1 M ratio of potassium hexacyanoferrate $K_4[Fe(CN)_6]$ was thoroughly mixed with either copper sulfate ($CuSO_4$) or nickel chloride ($NiCl_2$) at room temperature of 25 °C. Then a 0.1 M solution of NaOH and 50 g of RDP was added to the resulting suspensions. Lastly, the suspensions were centrifuged for 40 min. Then the supernatant was dried at 100 °C for 3 h. to obtain the RDP-FC-Cu and RDP-FC-Ni composite adsorbents. In the current study, the RDP, RDP-FC-Cu, and RDP-FC-Ni were stored in glass bottles to eliminate any contaminations for the batch adsorption experiments.

The date pits, roasted date pits, and the prepared composites were physiochemically characterized by previous work done by Al-Absi et al. (2021a,b). The study involved the utilization of various analytical techniques to investigate

the adsorptive capabilities and characteristics of the adsorbents. For the physical characterization of the adsorbents, particle size distribution (PSD) analysis, Brunauer–Emmett–Teller (BET) surface area and pore size analysis as well as scanning electron microscopy (SEM), were performed. Furthermore, the study involved the chemical characterization of the adsorbents utilizing thermogravimetric analysis (TGA), carbon and hydrogen analysis, Fourier-Transform Infrared Spectroscopy (FTIR) analysis, and X-ray diffraction (XRD).

2.2. Adsorption thermodynamic and isotherm studies

The SWRO brine sample was analyzed using ICP-OES analytical technique to ensure the presence of lithium ions. This is to confirm the main aim of this study, which is to effectively recover the industrially valuable metal from real SWRO desalination brine in Qatar. After detecting lithium ions and other metal ions in the SWRO brine, the adsorption studies were done as follows: synthetic solutions of lithium ions concentrations were prepared to test the adsorption capacities towards lithium ions without the interference of other metals. This was done by dissolving an amount of 0.6115 g of lithium chloride (LiCl) (Research-Lab Fine Industries, Mumbai 400 002 (India)) salt in 1L of distilled water (DW). The final concentration of the lithium ions was between 5 mg/L – 100 mg/L for the batch experiment. The experiment involved adding 50 mL of lithium ions solution of known initial concentration and a mass of 0.05 of the adsorbents (RDP, RDP-FC-Cu, or RDP-FC-Ni) into polycarbonate Erlenmeyer flasks. An incubator shaker was used to agitate the mixtures for 24 h. at 160 rpm at 25 °C, 35 °C, and 45 °C to study the effect of temperature on the adsorption capacities of lithium ions. Previous findings of Al-Absi et al. (2021a,b) revealed that the adsorption of lithium ions under the same conditions was the highest at a pH value of 6. Therefore, the pH of the solution was adjusted using minute amounts of 0.5 M NaOH and 0.5 M HCl solutions to be at a value of 6. After an equilibrium state was reached, filtration of the adsorbents was done using filter papers (0.2 μm). An ICP-OES analytical technique was used to analyze the residual concentration of lithium remaining in the solutions. The adsorption removal and capacity were obtained using Eqs. (1) and (2).

This provides an understanding of the adsorbent's capability of adsorbing a target pollutant in terms of a percentage (Pelalak et al., 2021).

$$\%\ \text{Removal} = \frac{C_i - C_e}{C_i} \times 100 \tag{1}$$

Where C_i is the initial concentration of the adsorbate (mg/L), and C_e is the concentration of the adsorbate at an equilibrium state (mg/L).

The adsorption capacity (qe) is defined as the quantity of adsorbate that an adsorbent can carry per unit mass of adsorbent. Eq. (2) represents the mathematical formula for the calculation of the adsorption capacity (Chowdhury et al., 2020).

$$q_{e=}\frac{(C_i - C_e)\,V}{m} \tag{2}$$

In Eq. (2), C_e and C_i are the equilibrium and initial lithium ions concentrations (mg/L), respectively. The volume of the solution (L) is expressed as V and the mass (g) of the material used is given the symbol of m.

Moreover, the adsorption thermodynamics is known as Gibbs free energy (ΔG^o), enthalpy (ΔH^o) and entropy (ΔS°) were calculated to understand the spontaneity, favorability, and whether the adsorption of lithium ions onto the prepared adsorbents is endothermic or exothermic. Eqs. (3) and (4) show Gibbs free energy as well as enthalpy and entropy calculations.

The calculation of Gibbs free energy for adsorption systems can be done through the following Eq. (3):

$$\Delta G^\circ = -RT\ lnk_L \tag{3}$$

where R is the universal gas constant of the value of 8.314 J/mol K, T is the absolute temperature in kelvins, and k_L is Langmuir isotherm constant, which can be expressed as standard enthalpy and entropy changes of adsorption as functions of temperature (Yadav et al., 2021).

The relationship between temperature and k_L is shown in the following formula known as Van't Hoff Eq. (4):

$$Lnk_L = \frac{-\Delta H^O}{R}\left(\frac{1}{T}\right) + \frac{\Delta S^O}{R} \tag{4}$$

where a plot of lnk $_L$ vs. T can be used to determine the values of ΔH° and ΔS° from the slope and intercept (Konicki et al., 2017).

The isotherm studies were established by fitting the data in the Langmuir, Freundlich, Dubinin–Radushkevich, and Temkin adsorption isotherm models. The adsorption parameters for the Langmuir and Freundlich fit were estimated by Eqs. (5) and (6), respectively. Similarly, the calculation of the adsorption parameters for Dubinin–Radushkevich was done using Eqs. (7), and (8). Eqs. (9) and (10) represent the calculation of the Temkin adsorption isotherm model's parameters.

To analyze Langmuir's adsorption model for a given adsorption process, the linear equation could be used (Eq. (5)) (Langmuir, 1916; Do, 1998):

$$\frac{C_e}{q_e} = \frac{C_e}{C_m} + \frac{1}{K_L C_m} \tag{5}$$

Where C_e is the equilibrium concentration (mg/L) of the adsorbate, the equilibrium adsorption capacity (mg/g) is q_e, the constant for the adsorption capacity for the formation of a monolayer in mg/g is C_m and the constant describes the adsorption sites affinity towards the adsorbate in L/mg is k_L (Weber and Chakravorti, 1974; Langmuir, 1918). The Langmuir plot between $\frac{C_e}{q_e} Vs. C_e$ provides the necessary values for the calculation of the Langmuir constants (k_L and C_m) through the slope and intercept (Ezzati, 2020; Apolinário and Pires, 2020).

Similar to Langmuir's adsorption isotherm model, the linear equation of the Freundlich model is shown in Eq. (6) below. The model plotted as ln (q_e) vs. ln (C_e) (Adamson and Gast, 1997; Zeldowitsch, 1934).

$$\log q_e = \log K_f + \frac{1}{n} \log C_e \tag{6}$$

Where q_e is the adsorption capacity in mg/g, the K_f is the model's constant in terms of mg/g, the level of deviation from linearity is n, and C_e is the equilibrium concentration of the adsorbate in mg/L (Chen et al., 2015; Do, 1998).

The following exponential formula (Eq. (7)) can be used to plot the Dubinin–Radushkevich adsorption isotherm as ln(q_e) vs. ε^2 (Hu and Zhang, 2019; Dubinin, 1960).

$$lnq_e = \ln X_m - B_{DR}\varepsilon^2 \tag{7}$$

where q_e is the amount of adsorbate adsorbed per gram of adsorbent at equilibrium in mg/g, X_m is the maximum adsorption capacity of the adsorbent, B_{DR} is the adsorption energy constant (mol ^{2}/kJ ^{2}), and ε is the Dubinin–Radushkevich isotherm constant represented by the following formula (Eq. (8)):

$$\varepsilon = RTln(1 + \frac{1}{C_e}) \tag{8}$$

where R is the universal gas constant of the value of 8.314 J/mol K, T is the temperature in Kelvin and C_e is the concentration of the adsorbate at equilibrium in mg/L (Hobson, 1969; Hu and Zhang, 2019).

The Temkin adsorption isotherm model can be plotted as q_e vs. ln C_e using the following linear form of the formula (Eq. (9)) (Nandiyanto et al., 2020; Aharoni and Ungarish, 1977):

$$q_e = B \ln A_T + B \ln C_e \tag{9}$$

where q_e is the amount of adsorbate adsorbed per gram of adsorbent at equilibrium in mg/g, C_e is the concentration of the adsorbate at equilibrium in mg/L, A_T is the Temkin isotherm equilibrium binding constant in L/g, and B is a constant related to the heat of sorption in J/mol. The constant B can be found using the following formula (Eq. (10)):

$$B = (\frac{RT}{b_T}) \tag{10}$$

Where R is the universal gas constant of the value of 8.314 J/mol K, T is the temperature in kelvins, and b_T is the Temkin isotherm constant (Ayawei et al., 2017; Vadi et al., 2013).

2.3. Desorption studies

The recovery of lithium ions and regeneration of the spent adsorbents (RDP, RDP-FC-Cu, and RDP-FC-Ni) would allow the multiple usages of the adsorbents for metal recovery. To recover the adsorbed metal from the adsorbents, 0.5M and 1M HCl solutions were used to determine the concentration that would achieve the highest desorption percentage (Chatterjee and Abraham, 2019). The spent adsorbents from the previous adsorption experiment will be dried on filter papers and collected for the desorption experiments. Specifically, all the spent adsorbents that were involved in the adsorption of lithium ions at the optimum found pH of 6, room temperature of 25 °C, and metal concentrations of (5, 10, 15, 20, 25, 30, 35, 50, 70, and 100) mg/L were dried and collected. Then, the collected date pits were put in polycarbonate Erlenmeyer flasks with 50 mL of 0.5 M and 1 M HCl solution. The solutions were put in an incubator shaker at 35 °C for 24 h. at 160 rpm. to reach the equilibrium desorption state. The adsorbent was then be filtered out using filters (0.2 μm). The residual metal concentration in the solution was analyzed using ICP-OES analytical technique. After that, the percentage desorption was calculated based on the initial average adsorbed lithium ions concentrations that were determined in the previous experiment. Eq. (11) shows the calculations of the percentage desorption at different HCl concentrations (Ivanets et al., 2021).

$$\%\ Desorption = \frac{Average\ adsorbed\ lithiumions\ concentration - desorbed\ lithiumions\ concentration}{average\ adsorbed\ lithiumions\ concentration} \times 100 \tag{11}$$

The concentrations in Eq. (11) above are in the unit of mg/L.

2.4. Selectivity study

The selectivity of the adsorbents (RDP, RDP-FC-Cu, and RDP-FC-Ni) towards lithium ions in the presence of other competing ions was tested using an RO seawater desalination brine sample. The brine sample was tested for the presence

and concentration of lithium ions by the ICP-OES analytical technique. The selectivity study was done by applying adsorption experiments to the collected reverse osmosis brine sample directly. As with the previous batch adsorption experiment, the selectivity experiment was done by adding 0.05 g of each adsorbent (RDP, RDP-FC-Cu, and RDP-FC-Ni) into a 50 mL of the RO brine sample in polycarbonate Erlenmeyer flasks. The solutions were then kept in an incubator shaker at 35 °C for 24 h. at 160 rpm. The adsorbents were then filtered out using filters (0.2 μm). The residual lithium ions concentrations in the solutions were analyzed using ICP-OES analytical technique. The temperature was chosen as 35 °C for two main reasons. First and as mentioned previously, reject brine streams are characterized by their warm temperatures. Therefore, if the results demonstrate high adsorption capacities, the adsorption process could be performed without extra modifications on the brine sample (in the form of adding or reducing adsorption process temperatures). Secondly, the results of the previous batch adsorption experiment showed that a temperature of 35 °C achieved high lithium adsorption onto the three adsorbents.

2.5. Adsorption mechanisms of lithium ions onto RDP, RDP-FC-Cu, and RDP-FC-Ni

An investigation of the specific and unique adsorbent–adsorbate interactions and adsorption mechanisms was done. The physiochemical characteristics of the adsorbents as well as the lithium ions were explored for their roles in the adsorption mechanisms. This allows for the optimization of adsorption processes as well as selecting the most effective adsorbent for lithium ions.

2.6. Cost analysis for the preparation of the adsorbents

A laboratory-based cost analysis was done to determine the total cost required to prepare the RDP, RDP-FC-Cu, and RDP-FC-Ni adsorbents. This would give insights regarding the feasibility of the study as well as the environmental effects and cost-efficiency.

3. Results and discussion

3.1. Physiochemical characterization of the prepared adsorbents

The three prepared adsorbents denoted as RDP, RDP-FC-Cu, and RDP-FC-Ni were physiochemically characterized by our previous work using various analytical techniques (Al-Absi et al., 2021a,b). This study overviews the most important findings regarding the adsorptive capabilities and potentials of the three adsorbents (Table 1). The SEM results showed significant changes on the surface of the three adsorbents when compared to the initial material of raw date pits. To illustrate, the RDP presented the formations of various cavities and elevated formations on its surface while the RDP-FC-Cu and RDP-FC-Ni showed enhanced morphological structures. The structures of the prepared composites showed denser, rougher, more porous, and more fractures on their surfaces. The main reasons behind these morphological changes are the addition of chemicals, stirring, and centrifuging during the preparation process. These morphological enhancements resulted in more pore filling of lithium ions onto the surface of the composite adsorbents (Zhang and Chen, 2020)

The particle size distribution (PSD) test revealed that the RDP-FC-Ni composite had the smallest particle sizes followed by RDP-FC-Cu and lastly, RDP. For RDP-F-Ni, 90% of the sample had particle sizes less than 804.3 μm while RDP-FC-Cu and RDP had particle sizes less than 906 and 1,159.6 μm. This result is predictable due to the fact that nickel has a smaller hydrated ionic radius than copper, which resulted in a smaller overall composite material (Zhuang and Wang, 2019). This overall smaller particle size of the RDP-FC-Ni was also shown by the BET results where had the largest surface area (5.3 m^2/g) followed by RDP-FC-Cu (4.7 m^2/g) and then RDP (2.5 m^2/g). However, the largest pore size was attributed to RDP-FC-Cu (138.6 A°) followed by RDP-FC-Ni (82 A°), and lastly, RDP (39.2 A°). For the pore volumes, RDP-FC-Cu had the deepest volume (0.032964 cc/g) while the RDP and RDP-FC-Ni had similar results. The carbon and nitrogen elemental analysis of the three prepared adsorbents showed that the two composites had more carbon and less nitrogen contents than the RDP, which is found by studies to be due to the chemical and thermal modifications (Alves et al., 2020). Interestingly, the prepared composites demonstrated more and unique functional groups than the RDP. The modification through hexacyanoferrates resulted in the formation of C≡N and Fe-O bonds in the composites, which confirmed the modification process (Long et al., 2020). Similar results were obtained by several studies done on the characterization of metal hexacyanoferrates through FTIR. For example, Ma et al. (2019) studied the functional groups present on synthesized copper hexacyanoferrates nanoflakes and found the presence of the C≡N functional group. Also, Chong and co-workers obtained similar results on the synthesized nickel hexacyanoferrate cathode batteries. Moreover, the RDP-FC-Ni showed the highest thermal stability followed by RDP-FC-Cu and RDP through the TGA. These results confirmed that modification of RDP to RDP-FC-Cu and RDP-FC-Ni using potassium metal hexacyanoferrates resulted in enhanced physicochemical characteristics and adsorption properties (Misra et al., 2020).

Table 1
Comparison of the RDP, RDP-FC-Cu and RDP-FC-Ni physiochemical characteristics.

Adsorbent	SEM	PSD	BET	CN	FTIR	TGA
RDP	Cavities and elevated formations	90% of sample <1159.6 μm	SA: 2.5 m^2/g Pore size: 39.2 A° Pore volume: 0.010325 cc/g	C: 37.42% N: 5.04%	Secondary amines, esters, alkenes, and polysaccharides	Lowest thermal stability
RDP-FC-Cu	Rough, dense, and porous fractures	90% of sample <906 μm	SA: 4.7 m^2/g Pore size: 138.6 A° Pore volume: 0.032964 cc/g	C: 45.75% N: 1.10%	Secondary amines, esters, alkenes, polysaccharides, C≡N, and Fe–O	Moderate thermal stability
RDP-FC-Ni		90% of sample <804.3 μm	SA: 5.3 m^2/g Pore size: 82 A° Pore volume: 0.010306 cc/g	C: 46.04% N: 1.07%		Highest thermal stability

3.2. Effect of temperature and thermodynamics on the adsorption of lithium ions onto roasted date pits and two composites

Temperature plays a significant role in adsorption systems. The efficiency and overall removal of pollutants and recovery of metals depend largely on the surrounding temperature of a batch adsorption process. In nature, some adsorption systems could be exothermic while others could be endothermic (Rizzi et al., 2017). For these reasons, it was vital to study the effect of temperature on the recovery of lithium ions onto RDP, RDP-FC-Cu, and RDP-FC-Ni. The adsorption batch tests of lithium ions onto the three adsorbents were performed at 25 °C, 35 °C, and 45 °C.

Figs. 1–3 show the adsorption capacities and efficiencies of lithium ions onto RDP, RDP-FC-Cu, and RDP-FC-Ni at a variety of temperatures. As a general trend for all adsorbents involved in the study, the adsorption of lithium ions is enhanced with an increase in temperature from 25 °C to 45 °C (P-value < 0.05). Furthermore, the highest adsorption capacities and efficiencies for lithium ions at a variety of temperatures were observed for RDP-FC-Cu followed by RDP-FC-Ni and RDP (P-value < 0.05). This is predictable as it was found previously that RDP-FC-Cu and RDP-FC-Ni are the most effective and selective adsorbents for lithium ions at a variety of pH ranges and initial concentrations.

The adsorption capacity of lithium ions at 5 mg/L onto RDP (Fig. 1A and B) is found to increase significantly from being equal to 1.33 mg/g (26.5%) at 25 °C to 2.37 mg/g (47.44%) at 35 °C and 4.13 mg/g (82.64%) at 45 °C (P-value < 0.05). Similar adsorption trends were observed for lithium ions concentrations below 35 mg/L. This is a typical adsorption behavior with the variating temperature at low lithium ions concentrations. Under these circumstances, the adsorption active binding sites are plentiful while the lithium ions' concentration is low, which means that mass transfer and internal diffusion forces are somewhat weak. Therefore, a higher temperature would facilitate the mass transfer process of lithium ions onto the internal pores of the adsorbent (Hou et al., 2020; Snyders et al., 2014; Ji et al., 2021). In other words, higher temperatures increase the rates of lithium ions movements as well as pore diffusions due to an increase in the energy of the system. An increase in solution temperature would mostly result in decreased solution viscosity, which enhances the diffusion forces of the pollutants onto the adsorption active binding sites of the adsorbent and facilitate lithium ions complexations and coordination (Wadhawan et al., 2020). However, at lithium ions concentrations of 35 mg/L and higher, the adsorption capacities and efficiencies of RDP became very similar at temperatures of 35 and 45 °C. These adsorption capacities and efficiencies were higher than the results obtained under 25 °C (P-value < 0.05). Also, the adsorption capacities and efficiencies are observed to increase at a slower rate at lithium ions concentrations above 30 mg/L. As the concentration of lithium ions increases in the solution, the available active binding sites decrease. Therefore, temperatures higher than 25 °C are required to facilitate the internal diffusion of lithium ions onto the pores of the date pits. However, the adsorption binding sites are finite, which causes a slower rate of increase in adsorption despite the increasing temperature. The similarity of the adsorption capacities and efficiencies of lithium ions at 35 and 45 °C at higher concentrations could be due to the high collisions and mass transfer forces that dominate in the solution, which resulted in the high and similar adsorption patterns at the moderate temperature of 35 °C when compared to 45 °C. It is worth noting that in adsorption systems, the removal of pollutants or metals proceeds until an equilibrium state is achieved (Albatrni et al., 2020; Saad et al., 2008). This means that the adsorption binding sites become fully filled or adsorption/desorption takes place at a constant and equilibrium state. This explains that despite the increase in temperature with concentration, the achieved adsorption capacity under 35 °C and 45 °C was similar. However, the temperature of 45 °C achieved the highest adsorption at all metal concentrations. This observation is of significant importance for scientists and environmentalists because it provides flexibility when optimizing an adsorption system for lithium ions recovery from brines. Raising the temperature requires energy and cost expenditure, which could be not feasible for some countries. Therefore, sufficient and efficient lithium recovery could be achievable at high concentrations and moderate temperatures of between 35 °C and 45 °C for RDP, while the highest recovery could be obtained at 45 °C. As mentioned previously, seawater reverse osmosis concentrated brine solutions are characterized by their high temperatures. Therefore, they could be utilized for metal recovery on a desalination plant for optimum and maximum recovery.

The adsorption of lithium ions onto RDP-FC-Cu (Fig. 2A and B) at a variety of temperatures (25, 35 and 45 °C) and concentrations (5, 10, 15, 20, 25, 30, 35, 50, 70, and 100) mg/L follows a similar trend to its adsorption onto RDP. However,

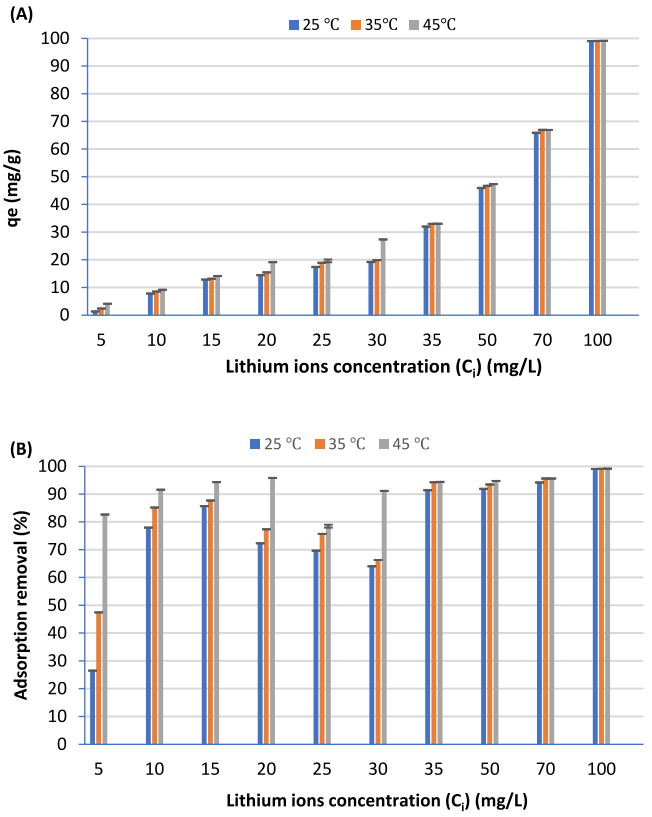

Fig. 1. The effect of temperature on the adsorption (A) capacity and (B) percent removal of lithium ions onto RDP. The experimental conditions were as follows: the adsorption batch tests of lithium onto the adsorbents were performed at 25, 35, and 45 °C and shaking time of 24 h. at 160 rpm. Also, the adsorbent mass was constant at 0.05 g, and the lithium concentrations were 2, 5, 10, 15, 20, 25, 30, 35, 50, 70, and 100 ppm in a total volume of 50 ml. The pH of the solution was kept constant at the optimum pH of 6. The error bars are shown in the figure.

the adsorption capacities and removals of RDP-FC-Cu are higher than RDP. The maximum adsorption of lithium ions took place when the temperature was raised to 45 °C for all initial metal concentrations with the highest adsorption achieved at 100 mg/L (Adsorption capacity of 99.3 mg/g). Also, the difference between the adsorption capacities/efficiencies at different temperatures was found to be significant (P-value < 0.05). Similar to RDP, higher differences between the adsorptions at 25 °C, 35 °C, and 45 °C were noticed at lithium ions concentrations below 30 mg/L. However, these differences in the adsorption of lithium ions at different temperatures are less evident than the differences observed for RDP. At higher lithium ions concentrations than 30 mg/L, the adsorption capacities and efficiencies were very similar for 35 and 45 °C. Interestingly, the RDP-FC-Cu composite showed significantly higher adsorption capacities and efficiencies for lithium ions at all temperatures than RDP and RDP-FC-Ni (Figs. 1 and 3). This adsorption behavior and favorability could be due to the previously mentioned exceptional and selective physiochemical characteristics of the adsorbent. The RDP-FC-Ni composite shows similar adsorption trends to RDP and RDP-FC-Cu in terms of increasing adsorption with temperature and concentration, higher differences in adsorption at low lithium ions concentrations, and similarity at high lithium ions concentration. RDP-FC-Ni (Fig. 3) showed higher adsorption capacities and efficiencies for lithium ions than RDP and lower than RDP-FC-Cu (P-value < 0.05). This could be due to the enhanced physicochemical characteristics for RDP-FC-Ni. However, RDP-FC-Cu shows a bigger pore radius and volume than RDP-FC-Ni, enhanced chemical characteristics, and functional groups. Furthermore, it is worth noting that the TGA results for RDP-FC-Cu revealed remarkable insights regarding its thermal stability. As mentioned previously, the thermal stability of adsorbents is of great importance for ensuring an optimized adsorption process. This is because temperature plays a significant role in the adsorption efficiency and capacity of numerous adsorbents. Many adsorption systems and in particular metal adsorptions require energy in terms of temperature increase to achieve high adsorption and recovery results (Albatrni et al., 2020). This study showed that the adsorption of lithium ions onto the three adsorbents favors increasing temperature. Therefore, the high thermal stability of RDP-FC-Cu explains its constant and relatively high adsorption capabilities towards lithium ions despite temperature changes. Moreover, the thermal stability of RDP-FC-Ni was found to be higher than RDP. This explains its higher adsorption capabilities than RDP. Similar results to the adsorption behaviors of lithium ions onto the three adsorbents at variating temperatures were obtained by many studies. For example, a study done by Yu et al. (2017) on the adsorption of gold onto chemically modified activated carbons revealed that the adsorption capacity increased with

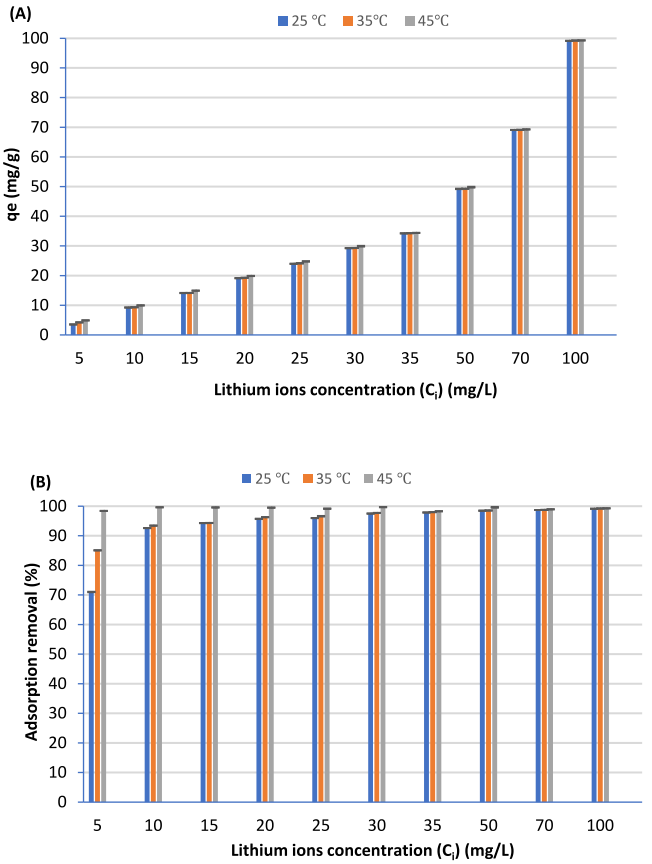

Fig. 2. The effect of temperature on the adsorption (A) capacity and (B) percent removal of lithium ions onto RDP-FC-Cu. The experimental conditions were as follows: the adsorption batch tests of lithium onto the adsorbents were performed at 25, 35, and 45 °C and shaking time of 24 h. at 160 rpm. Also, the adsorbent mass was constant at 0.05 g, and the lithium concentrations were 2, 5, 10, 15, 20, 25, 30, 35, 50, 70, and 100 ppm in a total volume of 50 ml. The pH of the solution was kept constant at the optimum pH of 6. The error bars are shown in the figure.

increasing temperature. This was due to enhanced internal diffusion onto the adsorbent. El-Bahy et al. (2018) showed that the adsorption of cesium ions onto a potassium copper hexacyanoferrate encapsulated carbomer favored increasing temperatures. The authors discussed the great role of temperature in the adsorption of metals from aqueous solutions. Increasing the temperature would lead to the increased kinetic energy of the system, which would, in turn, increase the mobility of metals and weaken their electrostatic repulsion forces, leading to higher collisions, and adsorption capacities. Another study performed by Naeimi and Faghihian (2017) discussed that the adsorption of cesium onto a modified potassium nickel hexacyanoferrate was an endothermic process that was continuously enhanced until an equilibrium was reached with an increase in temperature. Furthermore, Table 2 represents a comparison between the maximum adsorption capacities of different adsorbents towards lithium ions in solution. The high adsorption capacities achieved with the adsorbents at study show their extreme efficiencies and novelty of the work. This is because all synthesis of the adsorbents at study involved the utilization of readily available waste (Date pits) as well as cost-friendly and environmentally safe chemicals (Metal hexacyanoferrates).

3.2.1. Adsorption thermodynamics

Table 3 presents the enthalpy, entropy, and Gibbs free energy change values obtained for all the adsorbents involved in the study. As the previous experiment (effect of temperature on the adsorption of lithium ions onto the three adsorbents) indicated, the adsorption capacity increased with an increase of temperature from 25 to 45 °C for all adsorbents. This was confirmed by the positive values obtained for the enthalpy of all the adsorbents. This indicates that the adsorption of lithium ions onto the adsorbents is an endothermic process that requires the addition of energy (in the form of increased temperature) (Yadav et al., 2021; Aljerf, 2018). The values of the enthalpy were found to be equal to 140.12 kJ/mol, 336.73 kJ/mol, and 133.88 kJ/mol for RDP, RDP-FC-Cu, and RDP-FC-Ni, respectively. Furthermore, the Gibbs free energy values were found to be negative for all the adsorbents involved in the study. This means that the adsorption of lithium ions onto the adsorbents is a spontaneous and viable process. The Gibbs free energy values can be observed to decrease with increasing temperature, which indicates that the internal diffusion and mass transfer of lithium ions and adsorption are

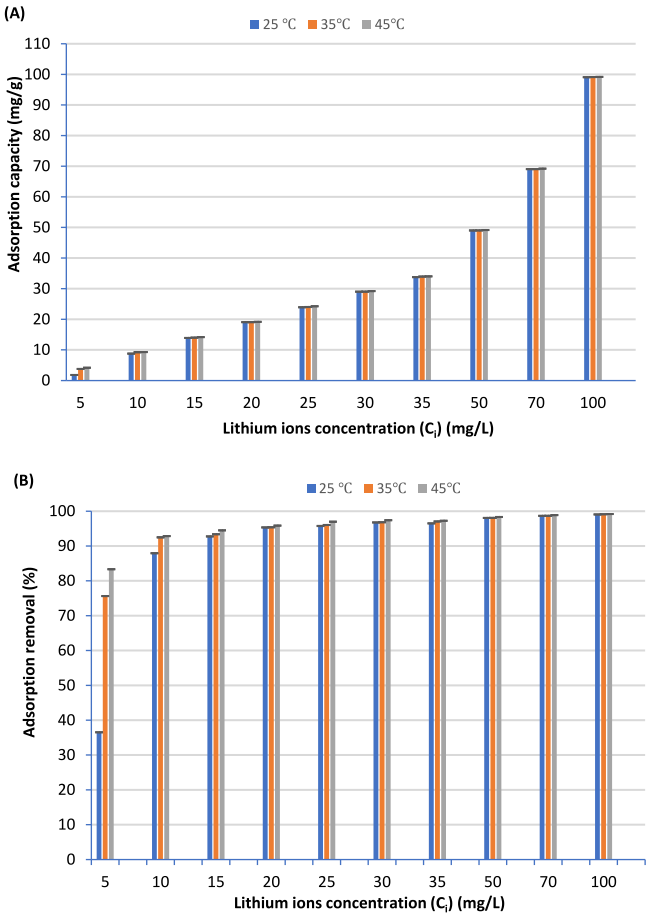

Fig. 3. The effect of temperature on the adsorption (A) capacity and (B) percent removal of lithium ions onto RDP-FC-Ni. The experimental conditions were as follows: the adsorption batch tests of lithium onto the adsorbents were performed at 25, 35, and 45 °C and shaking time of 24 h. at 160 rpm. Also, the adsorbent mass was constant at 0.05 g, and the lithium concentrations were 2, 5, 10, 15, 20, 25, 30, 35, 50, 70, and 100 ppm in a total volume of 50 ml. The pH of the solution was kept constant at the optimum pH of 6. The error bars are shown in the figure.

enhanced with temperature (Humelnicu et al., 2020). Lastly, the values of $\Delta S°$ give an understanding of the favorability of the adsorption process. The positive $\Delta S°$ values obtained for all adsorbents show that the adsorption of lithium ions is favorable for all the adsorbents involved in this study. Also, the adsorption process of lithium ions onto the adsorbents takes place with increased randomness and disorder (Aljerf, 2018). Similar results were obtained by Lawagon and co-workers who studied the adsorption of lithium ions onto H_2TiO_3. The study revealed that the adsorption process favored increasing temperature and was spontaneous from positive enthalpy and negative Gibbs free energy values, respectively. Another study done by Wahib et al. (2021) investigated the thermodynamics of the adsorption of lithium ions onto date pits (DP) impregnated with cellulose nanocrystals (CNCs) and ionic liquid (IL). The results revealed that the adsorption process was spontaneous from negative Gibbs free energy values. However, the enthalpy values of the study showed that the adsorption process was exothermic and is not affected by temperature. Moreover, the entropy values revealed that the adsorption of lithium ions does not favor a high level of disorder. A study done by Cheng and co-workers showed spontaneous and exothermic adsorption of lithium ions onto a chitosan nanofiber membrane. These studies show that the adsorption of lithium ions onto different adsorbents could result in different thermodynamic results. This shows the large impact that adsorbents pose on the feasibility of the adsorption process for the same pollutant. A study done by Zhou et al. (2017) on the adsorption of mercury onto modified graphene oxide revealed through the thermodynamic study that the process took place spontaneously and favorably with increasing temperature. On the other hand, Wadhawan et al. (2020) showed that mercury adsorption onto chitosan alginate nanoparticles decreased at temperatures above 30 °C, which indicated an exothermic adsorption process. This could be justified by the fact that some adsorbed metals would de-chelate or desorb at elevated temperatures due to specific adsorbent characteristics and increased mobility of the metal ions. Moreover, the adsorption of copper ions onto different adsorbents like magnetic, activated charcoal, and Na polymer-based composite of magnetic alginate was investigated by Yadav et al. (2021). Through the thermodynamic study, it was found that the adsorption process of copper was spontaneous, endothermic, and random.

Table 2
Comparison between the adsorption capacities of adsorbents.

Adsorbent	Initial Li^+ concentration (mg/L)	Adsorption capacity (mg/g)	Reference
Crown ether (CE) modified chitosan nanofiber membranes (CS-CE)	1000	297	Cheng et al. (2021)
Iron-doped lithium manganese oxide ion-sieve	50	34.8	Gao et al. (2021)
Crown ether polymeric microsphere porous adsorbents	80	2.31	Yuan et al. (2019)
Activated carbon modified with multiple MnO_2 ratios	20	88.5	Kamran et al. (2019)
Poly acrylic acid synthetic and natural zeolites	Synthetic Na-X zeolite with PAA: 1000 Natural clinoptilolite with PAA: 10	Synthetic Na-X zeolite with PAA: 0.5 Natural clinoptilolite with PAA: 5	Wiśniewska et al. (2018)
Nano-lithium-ion sieve	200	37.4	Tian et al. (2010)
1D LiMn2O4 nanorod	460	20	Zhang et al. (2010)
MnO2 ·0.4 H2O ion sieve	460	39.6	Xiao et al. (2015)
Date pits impregnated with cellulose nanocrystals and ionic liquid	100	99 mg/g	Wahib et al. (2021)
Roasted date pits	100	99.14	Current study
Roasted date pits modified with potassium copper hexacyanoferrate	100	99.3	Current study
Roasted date pits modified with potassium nickel hexacyanoferrate	100	99.18	Current study

Table 3
The adsorption enthalpy (ΔH^o), entropy (ΔS^o) and Gibbs free energy (ΔG^o) of lithium onto the adsorbents..

Adsorbent	ΔH^o (kJ/mol)		ΔS^o (J/K mol)
RDP	140.12		519.00
RDP-FC-Cu	336.73		1134.86
RDP-FC-Ni	133.88		449.90
ΔG^o (kJ/mol)			
Adsorbent	25 °C/298.15 K	35 °C/308.15 K	45 °C/318.15 K
RDP	−14.62	−19.81	−25.00
RDP-FC-Cu	−1.63	−12.97	−24.32
RDP-FC-Ni	−0.26	−4.76	−9.26

3.3. Adsorption isotherm models

The adsorption isotherm models can achieve an understanding of the specific adsorption mechanisms of metals and pollutants onto adsorbents. In addition, the unique interactions of pore filling between the adsorbate and adsorbent can be revealed by examining the adsorption isotherm models (Núñez-Gómez et al., 2019). Therefore, the most well-known and accepted adsorption isotherm models were conducted for the adsorption of lithium ions onto RDP, RDP-FC-Cu, and RDP-FC-Ni at variating temperatures (25 °C, 35 °C, and 45 °C) and metal concentrations (2, 5, 10, 15, 20, 25, 30, 35, 50, 70 and 100) mg/L. The applicability of the adsorption of lithium ions to Langmuir, Freundlich, Dubinin–Radushkevich, and Temkin's adsorption isotherm models was studied. The plots of the adsorption isotherm models reveal the linearity of the isotherm models as well as the R^2 values obtained for the recovery of lithium ions onto the three adsorbents.

Moreover, the adsorption isotherm model plots were used to calculate the isotherm-related constants for the three adsorbents involved in this study (Table 4) (Al-Ghouti and Al-Absi, 2020). All the adsorbents involved in the study showed R^2 values above 0.9 under the temperatures of 25 and 35 °C for the Langmuir adsorption isotherm model (Table 4). However, at 45 °C, the adsorption of lithium ions onto RDP-FC-Cu showed a 0.92 R^2 while the adsorption onto RDP and RDP-FC-Ni obtained lower R^2 values of 0.8 and 0.6, respectively. This means that at 25 °C and 35 °C, the adsorption of lithium ions onto RDP, RDP-FC-Cu, and RDP-FC-Ni follows monolayer adsorption. This means that the lithium ions would form a single layer only on the surface of the adsorbents at lower temperatures. However, at higher temperatures (45 °C), a monolayer adsorption mechanism is mainly achieved with RDP-FC-Cu (Al-Ghouti and Al-Absi, 2020). Table 3 shows the equation parameters of Langmuir adsorption isotherm that were calculated for the three adsorbents involved in this study. The monolayer adsorption capacity (C_m) values of RDP increased continuously when the temperature increased

Table 4
The equation parameters of the Langmuir, Freundlich, Dubinin–Raduchkevich, and Temkin isotherm models for the adsorption of lithium ions onto three adsorbents at a variety of initial lithium ions concentrations and temperatures.

Adsorbent	T (°C)	Langmuir			Freundlich			
		Monolayer adsorption capacity (Cm) (mg/g)	Favorability constant (k_L) (L/mg)	R^2	Adsorption constant (K_f) ((mg/g)/(g/L)$^{1/n}$)	Linearity deviation level (n)	1/n	R^2
RDP	25	17.86	7857	0.95	8.89	3.09	0.32	0.93
	35	19.61	1188	0.92	2.04	4.98	0.20	0.89
	45	22.37	500.5	0.80	2.31	5.08	0.20	0.88
	T (°C)	Temkin			Dubinin-Radushkevich			
		Equilibrium binding constant (A_T) (L/mg)	Heat of sorption constant (B) (J/mol)	R^2	Maximum adsorption capacity (X_m) (mg/g)	Adsorption energy constant (B_{DR}) (mol^2/KJ^2)	R^2	
	25	0.08	−34.6	0.83	27.0	4×10^{-7}	0.80	
	35	0.07	−36.1	0.90	17.2	5×10^{-7}	0.96	
	45	0.90	−179.3	0.33	39.2	-3×10^{-7}	0.90	
RDP-FC-Cu	T (°C)	Langmuir			Freundlich			
		Monolayer adsorption capacity (Cm) (mg/g)	Favorability constant (k_L) (L/mg)	R^2	Adsorption constant (K_f) ((mg/g)/(g/L)$^{1/n}$)	Linearity deviation level (n)	1/n	R^2
	25	1.780	4.240	0.96	13.48	0.31	3.21	0.82
	35	4.240	30.43	0.97	109.18	0.17	5.87	0.77
	45	38.91	22 889	0.92	110.30	0.59	1.69	0.91
	T (°C)	Temkin			Dubinin-Radushkevich			
		Equilibrium binding constant (A_T) (L/mg)	Heat of sorption constant (B) (J/mol)	R^2	Maximum adsorption capacity (Xm) (mg/g)	Adsorption energy constant (B_{DR}) (mol^2/KJ^2)	R^2	
	25	0.61	−39.0	0.86	1.3	4×10^{-7}	0.80	
	35	0.91	−81.3	0.44	6808.9	-1×10^{-6}	0.80	
	45	26.84	−26.08	0.80	59.4	-2×10^{-8}	0.80	
RDP-FC-Ni	T (°C)	Langmuir			Freundlich			
		Monolayer adsorption capacity (Cm) (mg/g)	Favorability constant (k_L) (L/mg)	R^2	Adsorption constant (K_f) (L/mg)	Linearity deviation level (n)	1/n	R^2
	25	4.970	29.71	0.94	35.88	0.42	2.39	0.78
	35	0.960	1.000	0.95	16.17	0.05	20.91	0.89
	45	2.700	7.880	0.60	39.82	0.22	4.45	0.95
	T (°C)	Temkin			Dubinin-Radushkevich			
		Equilibrium binding constant (A_T) (L/mg)	Heat of sorption constant (B) (J/mol)	R^2	Maximum adsorption capacity (Xm) (mg/g)	Adsorption energy constant (B_{DR}) (mol^2/KJ^2)	R^2	
	25	0.30	−12.15	0.83	1.24	1×10^{-6}	0.90	
	35	0.95	−465.88	0.80	31.7	2×10^{-6}	0.91	
	45	1.44	322.61	0.30	432.0	-7×10^{-7}	0.93	

from 25 °C to 45 °C. However, Langmuir's adsorption favorability constant (k_L) for RDP decreased continuously as the temperature increased from 25 °C to 45 °C. This stresses the great effect that temperature plays on the adsorption monolayer formations, favorability, and capacities of RDP (Zhang and Liu, 2020; Humelnicu et al., 2019). Similar trends in Langmuir's C_m values were obtained for the RDP-FC-Cu composite involved in the adsorption of lithium. Interestingly, For RDP-FC-Cu, the adsorption favorability values (k_L) continuously increased with the increase in temperature. Significant increases in the adsorption capacity and favorability values can be observed for RDP-FC-Cu when the temperature was increased to 45 °C. Along with the high R^2 obtained at 45 °C, this indicates that the highest and most favorable adsorption of lithium follows Langmuir's adsorption mechanism at 45 °C for RDP-FC-Cu (Yadav et al., 2021). For RDP-FC-Ni, the Langmuir's C_m and k_L values are found to decrease when the temperature was increased from 25 °C to 35 °C. However, at 45 °C Langmuir's adsorption capacity and favorability can be seen to increase for the adsorption of lithium ions onto RDP-FC-Ni.

The adsorption of lithium ions onto RDP at 25 °C followed Freundlich isotherm model best with an R^2 value of 0.93 (Table 4). At 35 and 45 °C, the adsorption of lithium ions onto RDP showed lower R^2 values of 0.89 and 0.88, respectively. It is worth noting that the adsorption of lithium ions at 25 °C could occur with the formation of monolayers and multilayers onto the surface of RDP. As the temperature increased to 35 and 45 °C, the adsorption mechanism of lithium ions onto RDP favored the formation of monolayers over multilayers. This is because the R^2 value obtained for RDP at 25 °C and 35 °C was higher for Langmuir's isotherm model (Table 4). For RDP-FC-Cu, the highest R^2 value for the Freundlich isotherm model was obtained at 45 °C ($R^2 = 0.91$) followed by 25 °C and then 35 °C (Table 4). A similar result is obtained with the adsorption of lithium ions onto RDP-FC-Ni, where the highest Freundlich R^2 value can be seen at 45 °C ($R^2 = 0.95$) but is followed by 35 and then 25 °C. Interestingly, the adsorption of lithium ions onto RDP-FC-Cu favored the monolayer formation over the multilayer mechanism at lower temperatures than 45 °C, with both mechanisms obtained at 45 °C. Similarly, the adsorption of lithium ions onto RDP-FC-Ni followed the Langmuir adsorption isotherm mechanism best at 25 and 35 °C with the formation of a multilayer adsorption mechanism at 45 °C. This shows the significant effect that temperature plays in variating the mechanism of lithium ions adsorption onto the studied adsorbents (Thanarasu et al., 2019). Furthermore, it is worth noting that the temperature which showed the highest adsorption capacity for lithium ions (45 °C) has also revealed shifts in the adsorption mechanisms. This temperature has caused the adsorption of lithium ions onto the adsorbents to take place as monolayer formations as well as multilayers, which indicates higher adsorption potentials and capacities due to mass transfer forces (Zhang and Liu, 2020; Borhade and Kale, 2017).

Freundlich adsorption isotherm parameters for RDP, RDP-FC-Cu, and RDP-FC-Ni are shown in Table 4. According to the results of the study, the adsorption of lithium ions onto RDP becomes more favorable, physical, and less cooperative in terms of Freundlich's isotherm model as the temperature increased from 25 °C to 45 °C. This is because the values for Freundlich's n are found to be higher than 1 and increase with temperature. Also, the values for $1/n$ are observed to be less than 1 and decrease with increasing temperature. Freundlich's adsorption capacity parameter is known as K_f, which is seen to decrease from 8.89 mg/g at 25 °C to 2.04 mg/g at 35 °C then increase at 45 °C to reach a value of 2.31 mg/g for RDP. To compare, the n and $1/n$ values for RDP-FC-Cu and RDP-FC-Ni reveal that the adsorption of lithium ions in terms of Freundlich's adsorption isotherm model could be a chemical cooperative process and is less efficient at low metal concentrations. Furthermore, the Freundlich adsorption capacity (K_f) values for RDP-FC-Cu are seen to continuously increase with temperature. On the other hand, the K_f values obtained for RDP-FC-Ni show that with the Freundlich isotherm mechanism, the adsorption capacity of lithium decreased as the temperature increased from 25 °C to 35 °C then increased as the temperature increased further to 45 °C. All in all, the applied adsorption isotherms indicate that the adsorption of lithium onto the three adsorbents at 25 °C and 35 °C could be more fitting to Langmuir's isotherm model than Freundlich model. At 45 °C, the adsorption of lithium ions onto RDP and RDP-FC-Cu could follow the Langmuir and the Freundlich adsorption mechanisms almost equally. However, the Freundlich adsorption isotherm model was found to be more fitting than Langmuir's model for the adsorption process of lithium ions onto RDP-FC-Ni at 45 °C.

Similar to Langmuir and Freundlich's adsorption isotherm analysis for the three adsorbents, Dubinin–Radushkevich was studied. Table 4 illustrates that all the adsorbents follow Dubinin–Radushkevich at all the studied temperatures to a good extent (R^2 values of 0.8 and higher). For RDP, the maximum adsorption capacity (Xm) can be found to decrease from 27 mg/g to 17.2 mg/g when the temperature was increased from 25 °C to 35 °C, then increase to the highest value (39.2 mg/g) at 45 °C. The highest adsorption energy (B_{DR}) value for RDP is for the adsorption at 35 °C followed by 25 °C then 45 °C. Moreover, the adsorption of lithium ions onto RDP was found to fit Temkin's adsorption isotherm model to a good extent at the temperatures of 25 °C and 35 °C. At those temperatures, the adsorption was found to be a physical and endothermic process. This is because the heat of adsorption constant (B) is negative at both temperatures. For RDP-FC-Cu, Dubinin–Radushkevich's maximum adsorption capacity (Xm) is the highest for 35 °C followed by 45 °C then 25 °C. However, the highest adsorption energy (B_{DR}) value for RDP-FC-Cu is for the adsorption at 25 °C followed by 35 °C then 45 °C. For RDP-FC-Ni, Dubinin–Radushkevich adsorption capacity (Xm) was found to increase with temperature. The adsorption energy constant (B_{DR}) was the highest for the adsorption at 35 °C followed by 25 °C then 45 °C. Furthermore, Temkin's adsorption isotherm model revealed that the adsorption of lithium onto RDP-FC-Ni is physical and endothermic at 25 °C and 35 °C.

3.4. Desorption of lithium ions from the roasted date pits and two composites

Investigators are often interested in the fate of the adsorbents that were involved in adsorption processes. After the uptake of a target pollutant such as metals from solutions, the adsorbent could be regenerated and reused by performing a desorption process (Gao et al., 2020). The main purpose for carrying on a desorption process is to re-use the adsorbent material for another adsorption process. Re-using the adsorbents as many times as possible is environmentally, sustainably, and economically important. This is because it would reduce the overall cost and waste materials in adsorption processes (Nur et al., 2018). For these reasons, desorption experiments using 1M and 0.5M HCl were done for lithium ions from the spent RDP, RDP-FC-Cu, and RDP-FC-Ni. Fig. 4 represents the percentage desorption achieved for lithium ions using 0.5M and 1M HCl, respectively. The results showed that all the adsorbents achieved similar adsorptions under the influence of 0.5M and 1M HCl. This demonstrates that there is no significant effect on the desorption efficiency between the two studied HCl concentrations (P-value > 0.05). Also, the high desorption efficiencies indicate that the adsorption of lithium ions onto the three adsorbents occurs due to the formations of weak and physical bonding (Ji et al.,

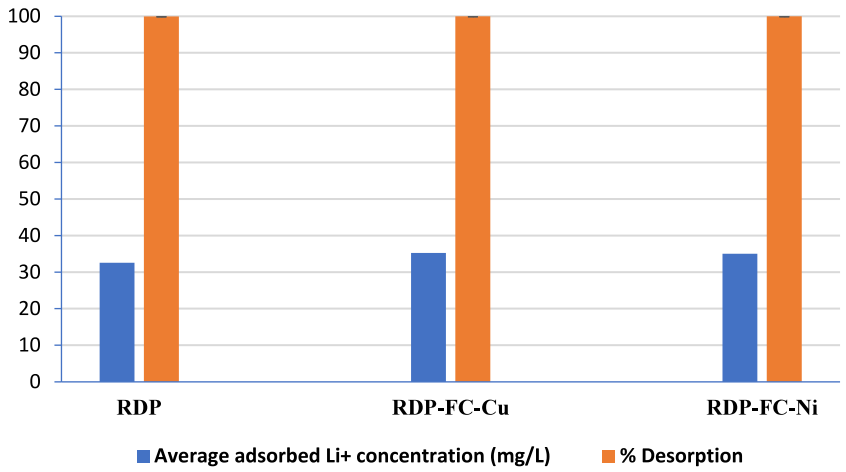

Fig. 4. The percentage desorption of the average adsorbed lithium ions concentration from RDP, RDP-FC-Cu, and RDP-FC-Ni using 0.5M and 1M HCl solution. The experimental conditions were as follows: temperature of 35 °C, shaking time of 24 h. at 160 rpm. The error bars are shown in the figure.

2021; Fan et al., 2021). Moreover, the three adsorbents could be effectively regenerated and re-used as 99.9% of the metal could be desorbed after the adsorption processes. This provides scientists with the extra benefit of harnessing the full adsorptive and functionality of the adsorbents before discarding them. In addition, and from an environmentally friendly perspective, the high desorption efficiencies for lithium ions from the three adsorbents would help lessen date pits wastes by re-using them.

3.5. Selective adsorption of lithium ions from the collected reverse osmosis brine

The presence of various metal species in brine streams could significantly affect the adsorption capacities of adsorbents towards target metals (Ryu et al., 2020). This is because some metals could compete for the available adsorption active sites present on the adsorbents. Additionally, some adsorbents would demonstrate certain physicochemical characteristics that would favor the adsorption of certain metals (Zhong et al., 2021). Therefore, it was vital to study the adsorption capabilities and selectivity of the RDP, RDP-FC-Cu, and RDP-FC-Ni towards lithium ions from the collected reverse osmosis brine sample. The adsorption temperature was set to 35 °C because of the reasons mentioned previously in the methodology. It was previously shown that the brine sample had a pH of around 7.8, which is close to the optimum pH chosen for the adsorption studies. Therefore, the real brine sample could be effectively used for the adsorption of valuable metals as soon as it is rejected from the desalination plant, which would provide various other industries with valuable metals for their productions. Table 5 represents the adsorbed concentrations of the various metals in the collected reverse osmosis brine sample by RDP, RDP-FC-Cu, and RDP-FC-Ni, respectively. As a general observation from Table 6, all adsorbents were capable of adsorbing the full amounts of barium, cesium, lanthanide, lead, vanadium, zinc, and strontium from the brine sample. For the other metals present in the brine sample, each metal showed unique adsorptive capabilities. For example, RDP was capable of adsorbing the highest amount of sodium and potassium followed by RDP-FC-Ni then RDP-FC-Cu. However, RDP-FC-Cu and RDP-FC-Ni achieved full recovery of calcium ions, while RDP adsorbed around 77 065 mg/L of the initial amount of 77 120 mg/L. Moreover, RDP-FC-Cu and RDP-FC-Ni achieved a higher and similar recovery of magnesium ions than RDP. For iron and lithium, both composites in the study showed a full recovery while RDP achieved recoveries of 24.85 mg/L and 43.85 mg/L from the initial amounts of 30.5 mg/L and 44.2 mg/L, respectively. Overall, RDP was capable of fully adsorbing 7 metals while RDP-FC-Cu and RDP-FC-Ni both adsorbed 10 metals of an initial amount of 13 metals. It is worth noting that both composites showed remarkable adsorption capabilities for the lithium ions. This demonstrates the great potential of the prepared composites in recovering and adsorbing various metals from the collected reverse osmosis brine sample. Table 6 shows the WHO discharge limits of the metals found in the RO desalination brine. It is important to limit and control their discharge into the environment (Shadman et al., 2019; Huang et al., 2021). Interestingly, the three adsorbents were capable of adsorbing the full amounts of barium, lead, vanadium, and zinc. As a result, non-adsorbed concentrations of these three metals are all below the WHO discharge limits (Table 6). In addition, the RDP-FC-Cu and RDP-FC-Ni were capable of adsorbing the full amounts of most of the other metals in the RO desalination brine, only leaving behind sodium and potassium. It is worth noting that the WHO did not establish guideline limits for potassium as it is considered a non-harmless metal. This demonstrates the remarkable adsorptive capabilities of the synthesized adsorbents towards lithium ions as well as the most toxic metals. Consequently, it can be concluded that the adsorption experiments are proven to be successful for recovering valuable metals efficiently and sustainably from reverse osmosis desalination brines.

Table 5
Comparison between the initial metal concentrations and the adsorbed concentrations from the collected reverse osmosis brine using RDP, RDP-FC-Cu, and RDP-FC-Ni.

Metal	Initial concentration (mg/L)	Concentration after adsorption (mg/L)	Adsorbed concentration (mg/L)	Remaining concentration after the adsorption process (mg/L)
	RDP			
Na^+	64 350	457	63 893	63 893
Ca^{2+}	77 120	54.57	77 065.43	77 065.43
K^+	151 300	111.8	151 188.2	151 188.2
Mg^{2+}	238 800	135.5	238 664.5	238 664.5
Ba^{2+}	3.3	<dl	3.3	≈0
Cs^+	3.4	<dl	3.4	≈0
In	4.5	<dl	4.5	≈0
Fe	30.5	5.65	24.85	24.85
Pb	10.1	<dl	10.1	≈0
Li^+	44.2	0.35	43.85	43.85
V	68.7	<dl	68.7	≈0
Zn^{2+}	256.4	<dl	256.4	≈0
Sr^{2+}	447	<dl	447	≈0
	RDP-FC-Cu			
Na^+	64 350	673.7	63 676.3	63 676.3
Ca^{2+}	77120	<dl	771,20	≈0
K^+	151 300	693.55	150 606.5	150 606.5
Mg^{2+}	238 800	37.53	238 762.5	238 762.5
Ba^{2+}	3.3	<dl	3.3	≈0
Cs^+	3.4	<dl	3.4	≈0
In	4.5	<dl	4.5	≈0
Fe	30.5	<dl	30.5	≈0
Pb	10.1	<dl	10.1	≈0
Li^+	44.2	<dl	44.2	≈0
V	68.7	<dl	68.7	≈0
Zn^{2+}	256.4	<dl	256.4	≈0
Sr^{2+}	447	<dl	447	≈0
	RDP-FC-Ni			
Na^+	64 350	592.84	63 757.16	63 757.16
Ca^{2+}	77 120	<dl	771,20	≈0
K^+	151 300	634.8	150 665.2	150 665.2
Mg^{2+}	238 800	33.62	238 766.4	238 766.4
Ba^{2+}	3.3	<dl	3.3	≈0
Cs^+	3.4	<dl	3.4	≈0
In	4.5	<dl	4.5	≈0
Fe	30.5	<dl	30.5	≈0
Pb	10.1	<dl	10.1	≈0
Li^+	44.2	<dl	44.2	≈0
V	68.7	<dl	68.7	≈0
Zn^{2+}	256.4	<dl	256.4	≈0
Sr^{2+}	447	<dl	447	≈0

<dl: Less than the detection limit.

Table 6
The WHO discharge limits of the metals found in the RO desalination brine sample.

Metal	WHO discharge limit (mg/L)	Reference
Na^+	500	WHO (1996)
Ca^{2+}	60	WHO (2011)
K^+	No limit established	
Mg^{2+}	250	WHO (2011)
Ba^{2+}	0.7	Yadav et al. (2019)
Cs^+	No limit established	
In	No limit established	
Fe	0.3	WHO (1996)
Pb	0.1	WHO (2011)
Li^+	1	Martone (2018)
V	0.1–1	WHO (2000)
Zn^{2+}	3	WHO (2011)
Sr2+	8	WHO (2010)

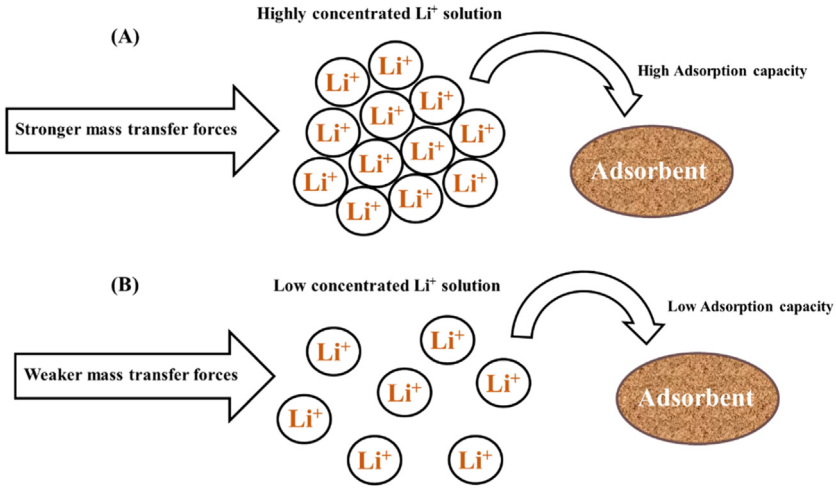

Fig. 5. (A) highly concentrated lithium ions solution would pose stronger mass transfer forces and higher adsorption capacity onto the adsorbent's surface and (B) low concentrated lithium ions solution would pose weaker mass transfer forces and lower adsorption capacity onto the adsorbent's surface.

3.6. The adsorption mechanisms of lithium ions onto RDP, RDP-FC-Cu, and RDP-FC-Ni

Establishing an understanding of the adsorption mechanisms of lithium ions onto the surface of RDP, RDP-FC-Cu, and RDP-FC-Ni is important for optimizing their removal process from brine streams. In adsorption systems, two main factors affect the adsorption capacity of pollutants. These two main factors are related to (i) the physiochemical characteristics of the adsorbents and (ii) the degree of affinity of the pollutant towards the adsorbent material (Al-Ghouti et al., 2010). These two factors often result in special interactions between the adsorbent and the adsorbate in solution and ultimately these interactions determine the level of adsorption potential or capacity (Fu et al., 2021). In adsorption systems, the driving force for molecules or ions onto the available active adsorption sites is internal diffusion from the highly concentrated solution to the low concentrated binding sites on the surface of the adsorbent (Albroomi et al., 2017). Therefore, at increasing initial lithium ions concentration in the solution, the collision and mass transfer forces dominated, which resulted in enhanced internal diffusion and adsorption capacities (El-Bahy et al., 2018). Moreover, it is important to note that factors like pH, temperature, adsorbent dosage, and particle size largely affect the collision and mass transfer forces (Kim et al., 2017a,b). This explains the enhanced adsorption capacities and efficiencies of lithium ions with increasing temperature as well as initial metal concentration. After the metal collides and reaches the surface of the adsorbent, various adsorption, and interaction mechanisms could take place (Al-Ghouti et al., 2010).

The mechanism of lithium ions adsorption onto RDP involves the interaction of lithium ions with the physio-chemical characteristics of the adsorbent. In adsorption systems that involve metal removal, the hydrated ionic radius of the metal plays a significant role in its adsorption capacity onto the available active sites of the adsorbent. To illustrate, the highest adsorption capacity is usually attributed to metals with the smallest hydrated radius due to the shorter distance between the adsorbent's surface and the metal (Naidu et al., 2016). The concentration of the metal ions plays a role in this case where higher metal concentration and lower hydrated radius would facilitate the faster and greater mass transfer, as well as adsorption potential between the adsorbent and the metal (Fig. 5). Moreover, the surface area, pore radius and pore volumes of the adsorbents involved in an adsorption process determine the affinity of the metal ion towards the available active sites (Zhuang and Wang, 2019). According to a study done by Al-Absi et al. (2021a,b), the BET pore radius and volume of RDP were equal to 39.2 Angstrom (Å) and 0.010325 cc/g, respectively. The BET pore radius and volume of RDP-FC-Cu were equal to 138.6 A and 0.032964 cc/g, respectively. On the other hand, RDP-FC-Ni had a pore radius of 82 Å and a pore volume of 0.010306 cc/g. To compare, lithium ions have a hydrated radius of only 3.4 Å. The adsorption experiments revealed that the highest adsorption of lithium ions was attributed to RDP-FC-Cu followed by RDP-FC-Ni with similar results at high initial concentrations and lastly, RDP. These findings are logical due to the physical characteristics of the available active sites on these three adsorbents and the hydrated ionic radius of lithium ion. The RDP-FC-Cu has the largest pore radius and volume when compared to the RDP and RDP-FC-Ni. However, the pore volume of RDP-FC-Ni was significantly larger than RDP. This means that more lithium ions were able to fill and penetrate deeper into the larger pores of RDP-FC-Cu and RDP-FC-Ni than RDP. The SEM of a study confirmed these findings of pore fillings where the pores and cavities of the RDP-FC-Cu appeared to significantly flatten and disappear upon the adsorption of lithium ions (Al-Absi et al., 2021a,b). Similar results were found for the adsorption of lithium ions onto RDP and RDP-FC-Ni, however, their surfaces were less affected by the adsorption process.

Roasted date pits are mainly composed of hemicelluloses, lignin, and celluloses (Mohammed et al., 2015). According to a previous study done by Al-Absi et al. (2021a,b), the main functional groups that were involved in the adsorption of lithium

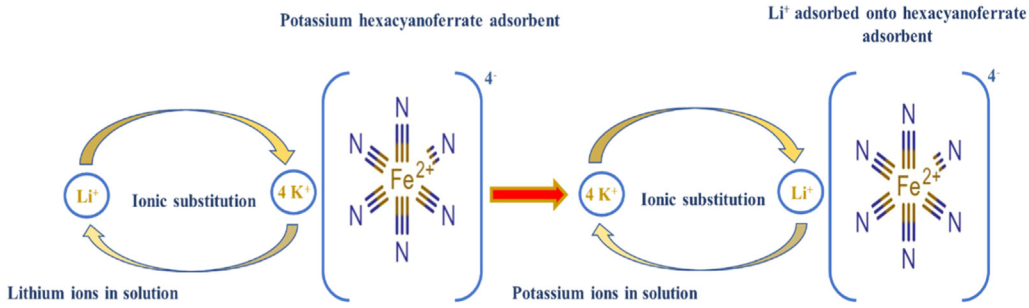

Fig. 6. The ionic substitution mechanism between lithium ions from a solution and potassium present in a potassium hexacyanoferrate-based adsorbent.

Table 7
The cost analysis for the RDP, RDP-FC-Cu, and RDP-FC-Ni adsorbents preparation.

Item	Unit cost (USD)	Amount used	Cost (USD)
Sodium hydroxide (1 kg)	40.49	1 g	1.21
Potassium hexacyanoferrate (500 g)	194.82	42.439 g	16.53
Copper sulfate (250 g)	49	7.98 g	1.56
Nickel chloride (250 g)	157	11.9 g	7.47
Total cost for grinding, roasting, and centrifuging	0.036 per kWh	8.40 kWh (100 °C; 24 h.), (Energy to Heat at 100 °C = 0.35 kWh/h)	0.302
Net cost			27.1
Other overhead costs (10% of the net cost)			2.71
Total cost			**29.81**

ions onto RDP were O-H, CHO, C=O, and polysaccharides. These functional groups were directly involved in the uptake of lithium ions as the FTIR spectrum showed band stretching and higher absorbance upon the adsorption process. Prior to the adsorption process, the FTIR intensity of these functional groups was much less than after the adsorption process. Studies have shown that the adsorption of metals onto RDP involves the fixation of the metal ions onto the cellulose-OH sites as well as the lignin-OH sites (Al-Ghouti et al., 2010). For RDP-FC-Cu and RDP-FC-Ni, the FTIR spectrum results demonstrated that the same functional groups were involved in the adsorption process as RDP. However, characteristic functional groups of C≡N were directly altered in terms of increased intensity upon the adsorption of lithium ions onto the two composite adsorbents. This shows that the mechanism of lithium ions adsorption onto the three adsorbents could be chemically different and unique to their chemical characteristics (Al-Absi et al., 2021a,b)

Furthermore, it is well-established that the main adsorption mechanism of metals onto metal hexacyanoferrates involves an ionic substitution between the target metal and the metal in the complex. To illustrate, metal hexacyanoferrates contain transition metals such as iron, copper, nickel, and potassium. Metals present in the adsorption solution could typically substitute the metals present in the hexacyanoferrate complex, typically due to their characteristics. The ionic substitution mechanism depends on the similarity of the characteristics between the target metal and the complex metal (Fig. 6) (Michel et al., 2015). In this study, it was shown that RDP-FC-Cu achieved the highest adsorption removal of lithium ions followed by RDP-FC-Ni and then RDP. The RDP-FC-Cu and RDP-FC-Ni have compromised roasted date pits-potassium copper or nickel hexacyanoferrate. The hydrated ionic radius of potassium is equal to 3.31 Å while it is equal to 1.98 Å for nickel and 4.19 Å for copper (Wang et al., 2018). Comparing these values with the hydrated ionic radius of lithium ion, it can be seen that it is closest to the hydrated radius of potassium followed by copper and then nickel. This means that lithium ions (in solution) were capable of substituting potassium in the two composites effectively. However, the slightly higher adsorption capacity achieved with RDP-FC-Cu is due to the close hydrated ionic radius of lithium and copper.

3.7. Cost-analysis of adsorbents preparation

Determining the overall cost of adsorbents preparation is important as it helps in decision making, optimizing procedures, and predicting any possible environmental impacts. In addition, the feasibility of the preparation processes could be analyzed for further improvements. The cost analysis of the preparation of the adsorbent was done based on a laboratory scale and is presented in Table 7. From the results, it can be concluded that the total cost of preparing 50 grams of each RDP, RDP-FC-Cu, and RDP-FC-Ni is around 29.81 USD. This amount was sufficient to perform all the experiments of this study as well as a previous study investigating the effect of pH and concentration on the adsorption of lithium ions from SWRO Qatari brine (Al-Absi et al., 2021a,b).

Conclusion

Recently, there has been a growing interest in recovering valuable metals from seawater desalination brines. One of the most cost-effective and environmentally friendly methods for metal recovery is adsorption. This study involved the usage of date pits and date pit-based metal hexacyanoferrates as cheap and readily available adsorbents for the adsorption of valuable lithium ions from seawater desalination brine. The results revealed that the adsorption process favored increasing concentration, temperature, and was endothermic, spontaneous, favorable, and followed all isotherm models at specific temperatures. The highest adsorption capacity of lithium ions was attributed to the RDP-FC-Cu with similar results to RDP-FC-Ni at high concentrations (100 mg/L) and temperature (45 °C). Moreover, the mechanism of lithium ions adsorption was unique to each adsorbent where the physicochemical characteristics of the adsorbents played a significant role. These characteristics included the surface area, pore size, and volumes as well as functional groups. The metal's hydrated ionic radius was a contributing factor in determining the adsorption mechanism. Also, the higher adsorption capacity achieved for RDP-FC-Cu when compared to RDP and RDP-FC-Ni was due to many factors, but mainly the similar hydrated ionic radius of lithium, copper, and potassium. This has allowed lithium ions to effectively substitute copper and potassium in the RDP-FC-Cu composite. The RDP-FC-Ni achieved better adsorption capacities for lithium ions than RDP due to the increased surface area, pore size, and volumes as well as high functionality of the adsorbent. Furthermore, a cost analysis for the preparation of the adsorbent was done and revealed that a total of 29.81 USD is required to prepare 50 g of each adsorbent.

CRediT authorship contribution statement

Rana S. Al-Absi: Formal analysis, Methodology, Validation, Writing – review & editing. **Mohammed H. Abu-Dieyeh:** Conceptualization, Supervision, Visualization, Methodology, Validation, Writing – review & editing. **Radhouane Ben-Hamadou:** Methodology, Validation, Writing – review & editing. **Mustafa S. Nasser:** Methodology, Validation, Writing – review & editing. **Mohammad A. Al-Ghouti:** Conceptualization, Supervision, Visualization, Methodology, Validation, Writing – review & editing.

Declaration of competing interest

The authors declare that they have no known competing financial interests or personal relationships that could have appeared to influence the work reported in this paper.

Acknowledgment

This work was made possible by Qatar University collaborative internal grant # [QUCG-CAS-20/21-2]. The findings achieved herein are solely the responsibility of the author[s].

References

Adamson, A., Gast, A., 1997. Physical Chemistry of Surfaces, sixth ed. J. Wiley & Sons, New York, pp. 1–808.

Aharoni, C., Ungarish, M., 1977. Kinetics of activated chemisorption. Part 2.—theoretical models. J. Chem. Soc. Faraday Trans. 1: Phys. Chem. Condens. Phases 73, 456.

Al-Absi, R., Abu-Dieyeh, M., Al-Ghouti, M., 2021a. Brine management strategies, technologies, and recovery using adsorption processes. Environ. Technol. Innov. 22, 101541. http://dx.doi.org/10.1016/j.eti.2021.101541.

Al-Absi, R.S., Abu-Dieyeh, M.H., Ben-Hamadou, R., Nasser, M.S., Al-Ghouti, M.A., 2021b. Novel composite materials of modified roasted date pits using ferrocyanides for the recovery of lithium ions from seawater reverse osmosis brine. Sci. Rep. 11 (1), http://dx.doi.org/10.1038/s41598-021-98438-2.

Al-Ghouti, M., Al-Absi, R., 2020. Mechanistic understanding of the adsorption and thermodynamic aspects of cationic methylene blue dye onto cellulosic olive stones biomass from wastewater. Sci. Rep. 10 (1), http://dx.doi.org/10.1038/s41598-020-72996-3.

Al-Ghouti, M., Da'ana, D., Abu-Dieyeh, M., Khraisheh, M., 2019. Adsorptive removal of mercury from water by adsorbents derived from date pits. Sci. Rep. 9 (1), http://dx.doi.org/10.1038/s41598-019-51594-y.

Al-Ghouti, M., Li, J., Salamh, Y., Al-Laqtah, N., Walker, G., Ahmad, M., 2010. Adsorption mechanisms of removing heavy metals and dyes from aqueous solution using date pits solid adsorbent. J. Hard Mater. 176 (1–3), 510–520. http://dx.doi.org/10.1016/j.jhazmat.2009.11.059.

Albatrni, H., Qiblawey, H., El-Naas, M., 2020. Comparative study between adsorption and membrane technologies for the removal of mercury. Sep. Purif. Technol. 257, 117833. http://dx.doi.org/10.1016/j.seppur.2020.117833.

Albroomi, I.H., Elsayed, A.M., Baraka, A., Abdelmaged, A.M., 2017. Batch and fixed-bed adsorption of tartrazine azo-dye onto activated carbon prepared from apricot stones. Appl. Water Sci. 7, 2063–2074.

Alves, A., Martorano, L., Florentino, G., Lasmar, D., Miranda, Í., Lisboa, L., da Silva Chaar, J., 2020. Thermal diagnosis of heat conduction and combustion time of fruits of the Brazil nut tree (Bertholletia excelsa Bonpl.). Adv. Biosci. Biotechnol. 11 (02), 60–71. http://dx.doi.org/10.4236/abb.2020.112005.

Apolinário, F., Pires, A., 2020. Oil displacement by multicomponent slug injection: An analytical solution for langmuir adsorption isotherm. J. Pet. Sci. Eng. 107939. http://dx.doi.org/10.1016/j.petrol.2020.107939.

Ayawei, N., Ebelegi, A., Wankasi, D., 2017. Modelling and interpretation of adsorption isotherms. J. Chem. 2017, 1–11. http://dx.doi.org/10.1155/2017/3039817.

Baalousha, H., Ouda, O., 2017. Domestic water demand challenges in Qatar. Arab. J. Geosci. 10 (24), http://dx.doi.org/10.1007/s12517-017-3330-4.

Borhade, V.A., Kale, S.A., 2017. Calcined eggshell as a cost effective material for removal of dyes from aqueous solution. Applied Water Sciences 7 (8), 4255–4268.

Can, N., Ömür, B., Altındal, A., 2016. Modeling of heavy metal ion adsorption isotherms onto metallophthalocyanine film. Sensors Actuators B 237, 953–961. http://dx.doi.org/10.1016/j.snb.2016.07.026.
Chatterjee, A., Abraham, J., 2019. Desorption of heavy metals from metal loaded sorbents and e-wastes: A review. Biotechnol. Lett. 41 (3), 319–333. http://dx.doi.org/10.1007/s10529-019-02650-0.
Chen, X., Wang, Y., Liu, L., Cui, J., Gan, M., Shum, D., Chan, R., 2015. The effect of implementation intention on prospective memory: A systematic and meta-analytic review. Psychiatry Res. 226 (1), 14–22. http://dx.doi.org/10.1016/j.psychres.2015.01.011.
Cheng, Q., Zhang, Y., Zheng, X., Sun, W., Li, B., Wang, D., Li, Z., 2021. High specific surface crown ether modified chitosan nanofiber membrane by low-temperature phase separation for efficient selective adsorption of lithium. Sep. Purif. Technol. 262, 118312. http://dx.doi.org/10.1016/j.seppur.2021.118312.
Chowdhury, A., Kumari, S., Khan, A., Chandra, M., Hussain, S., 2020. Activated carbon loaded with Ni-Co-S nanoparticle for superior adsorption capacity of antibiotics and dye from wastewater: Kinetics and isotherms. Colloids Surf. A 125868. http://dx.doi.org/10.1016/j.colsurfa.2020.125868.
Darwish, M., Hassabou, A., Shomar, B., 2013. Using Seawater Reverse Osmosis (SWRO) desalting system for less environmental impacts in Qatar. Desalination 309, 113–124. http://dx.doi.org/10.1016/j.desal.2012.09.026.
Do, D., 1998. Adsorption analysis: equilibria and kinetics. Ser. Chem. Eng. 2, 1–916.
Dubinin, M., 1960. The potential theory of adsorption of gases and vapors for adsorbents with energetically nonuniform surfaces. Chem. Rev. 60 (2), 235–241. http://dx.doi.org/10.1021/cr60204a006.
El-Bahy, S., Fadel, D., El-Bahy, Z., Metwally, A., 2018. Rapid and highly efficient cesium removal by newly synthesized carbomer encapsulated potassium copper hexacyanoferrate composite. J. Environ. Chem. Eng. 6 (2), 1875–1885. http://dx.doi.org/10.1016/j.jece.2018.02.030.
Elsaid, K., Sayed, E., Abdelkareem, M., Baroutaji, A., Olabi, A., 2020. Environmental impact of desalination processes: Mitigation and control strategies. Sci. Total Environ. 740, 140125. http://dx.doi.org/10.1016/j.scitotenv.2020.140125.
Ezzati, R., 2020. Derivation of pseudo-first-order, pseudo-second-order and modified pseudo-first-order rate equations from langmuir and freundlich isotherms for adsorption. Chem. Eng. J. 392, 123705. http://dx.doi.org/10.1016/j.cej.2019.123705.
Fan, X., Ma, Z., Zou, Y., Liu, J., Hou, J., 2021. Investigation on the adsorption and desorption behaviors of heavy metals by tire wear particles with or without UV ageing processes. Environmental Research 195, 110858. http://dx.doi.org/10.1016/j.envres.2021.110858.
Fu, L., Li, J., Wang, G., Luan, Y., Dai, W., 2021. Adsorption behavior of organic pollutants on microplastics. Ecotoxicol. Environ. Saf. 217, 112207. http://dx.doi.org/10.1016/j.ecoenv.2021.112207.
Gao, J., Du, Z., Zhao, Q., Guo, Y., Cheng, F., 2021. Enhanced li+ adsorption by magnetically recyclable iron-doped lithium manganese oxide ion-sieve: Synthesis, characterization, adsorption kinetics and isotherm. J. Mater. Res. Technol. 13, 228–240. http://dx.doi.org/10.1016/j.jmrt.2021.04.073.
Gao, X., Liu, J., Li, M., Guo, C., Long, H., Zhang, Y., Xin, L., 2020. Mechanistic study of selective adsorption and reduction of Au (III) to gold nanoparticles by ion-imprinted porous alginate microspheres. Chemical Engineering Journal 385, 123897. http://dx.doi.org/10.1016/j.cej.2019.123897.
Gaztañaga, F., Sandoval, M., Luna, C., Jasen, P., 2020. Theoretical study about alkali metal adsorption on pristine and defective (8, 0) SWCNT: Geometrical, magnetic and electronic changes. Appl. Surf. Sci. 513, 145769. http://dx.doi.org/10.1016/j.apsusc.2020.145769.
Habiyaremye, A., 2020. Water innovation in South Africa: Mapping innovation successes and diffusion constraints. Environ. Sci. Policy 114, 217–229. http://dx.doi.org/10.1016/j.envsci.2020.08.011.
Hobson, J., 1969. Physical adsorption isotherms extending from ultrahigh vacuum to vapor pressure. J. Phys. Chem. 73 (8), 2720–2727. http://dx.doi.org/10.1021/j100842a045.
Hou, Q., Zhou, H., Zhang, W., Chang, Q., Yang, J., Xue, C., Hu, S., 2020. Boosting adsorption of heavy metal ions in wastewater through solar-driven interfacial evaporation of chemically-treated carbonized wood. Sci. Total Environ. 759, 144317. http://dx.doi.org/10.1016/j.scitotenv.2020.144317.
Hu, Q., Zhang, Z., 2019. Application of Dubinin–Radushkevich isotherm model at the solid/solution interface: A theoretical analysis. J. Molecular Liquids 277, 646–648. http://dx.doi.org/10.1016/j.molliq.2019.01.005.
Huang, Z., Liu, K., Duan, J., Wang, Q., 2021. A review of waste-containing building materials: Characterization of the heavy metal. Constr. Build. Mater. 309, 125107. http://dx.doi.org/10.1016/j.conbuildmat.2021.125107.
Humelnicu, D., Lazar, M., Ignat, M., Dinu, I., Dragan, E., Dinu, M., 2019. Removal of heavy metal ions from multi-component aqueous solutions by eco-friendly and low-cost composite sorbents with anisotropic pores. Journal Of Hazardous Materials 381, 120980. http://dx.doi.org/10.1016/j.jhazmat.2019.120980.
Humelnicu, D., Lazar, M., Ignat, M., Dinu, I., Dragan, E., Dinu, M., 2020. Removal of heavy metal ions from multi-component aqueous solutions by eco-friendly and low-cost composite sorbents with anisotropic pores. J. Hard Mater. 381, 120980. http://dx.doi.org/10.1016/j.jhazmat.2019.120980.
Ibrahim, H., Eltahir, E., 2019. Impact of brine discharge from seawater desalination plants on Persian/Arabian gulf salinity. J. Environ. Eng. 145 (12), 04019084. http://dx.doi.org/10.1061/(asce)ee.1943-7870.0001604.
Ivanets, A., Prozorovich, V., Kouznetsova, T., Dontsova, T., Yanushevska, O., Hosseini-Bandegharaei, A., et al., 2021. Effect of Mg2+ ions on competitive metal ions adsorption/desorption on magnesium ferrite: Mechanism, reusability and stability studies. J. Hard Mater. 411, 124902. http://dx.doi.org/10.1016/j.jhazmat.2020.124902.
Ji, C., Wu, D., Lu, J., Shan, C., Ren, Y., Li, T., et al., 2021. Temperature regulated adsorption and desorption of heavy metals to A-MIL-121: Mechanisms and the role of exchangeable protons. Water Research 189, 116599. http://dx.doi.org/10.1016/j.watres.2020.116599.
Kamran, U., Heo, Y., Lee, J., Park, S., 2019. Chemically modified activated carbon decorated with MnO2 nanocomposites for improving lithium adsorption and recovery from aqueous media. J. Alloys Compd. 794, 425–434. http://dx.doi.org/10.1016/j.jallcom.2019.04.211.
Kim, Y., Kim, Y., Kim, S., Harbottle, D., Lee, J., 2017a. Nanostructured potassium copper hexacyanoferrate-cellulose hydrogel for selective and rapid cesium adsorption. Chem. Eng. J. 313, 1042–1050.
Kim, Y., Kim, Y., Kim, S., Harbottle, D., Lee, J., 2017b. Nanostructured potassium copper hexacyanoferrate-cellulose hydrogel for selective and rapid cesium adsorption. Chem. Eng. J. 313, 1042–1050. http://dx.doi.org/10.1016/j.cej.2016.10.1361385-894.
Kim, C.Y., Min, T., 2020. Influence of osmotic mediation on permeation of water in reverse osmosis: Experimental and numerical analysis. J. Membrane Sci. 595, 117574. http://dx.doi.org/10.1016/j.memsci.2019.117574.
Kim, J., Park, K., Yang, D., Hong, S., 2019. A comprehensive review of energy consumption of seawater reverse osmosis desalination plants. Appl. Energy 254, 113652. http://dx.doi.org/10.1016/j.apenergy.2019.113652.
Konicki, W., Aleksandrzak, M., Mijowska, E., 2017. Equilibrium, kinetic and thermodynamic studies on adsorption of cationic dyes from aqueous solutions using graphene oxide. Chem. Eng. Res. Des. 123, 35–49.
Langmuir, I., 1916. The constitution and fundamental properties of solids and liquids. Part I. Solids. J. Am. Chem. Soc. 38 (11), 2221–2295.
Langmuir, I., 1918. The adsorption of gases on plane surfaces of glass, mica and platinum. J. Am. Chem. Soc. 40 (9), 1361–1403. http://dx.doi.org/10.1021/ja02242a004.
Lee, K., Jepson, W., 2021. Environmental impact of desalination: A systematic review of Life Cycle Assessment. Desalination 509, 115066. http://dx.doi.org/10.1016/j.desal.2021.115066.
Long, X., Chen, R., Tan, J., Lu, Y., Wang, J., Huang, T., Lei, Q., 2020. Electrochemical recovery of cobalt using nanoparticles film of copper hexacyanoferrates from aqueous solution. J. Hard Mater. 384, 121252. http://dx.doi.org/10.1016/j.jhazmat.2019.121252.
Ma, X., Jia, W., Wang, J., Zhou, J., Wu, Y., Wei, Y., et al., 2019. Synthesis of copper hexacyanoferrate nanoflake as a cathode for sodium-ion batteries. Ceram. Int. 45 (1), 740–746. http://dx.doi.org/10.1016/j.ceramint.2018.09.238.

Mannan, M., Alhaj, M., Mabrouk, A., Al-Ghamdi, S., 2019. Examining the life-cycle environmental impacts of desalination: A case study in the State of Qatar. Desalination 452, 238–246. http://dx.doi.org/10.1016/j.desal.2018.11.017.
Martone, G., 2018. Nutritional lithium. J. Clin. Psychiatry Neurosci. 1 (1), 3–4.
Michel, C., Barré, Y., de Dieuleveult, C., Grandjean, A., De Windt, L., 2015. Cs ion exchange by a potassium nickel hexacyanoferrate loaded on a granular support. Chem. Eng. Sci. 137, 904–913.
Misra, N., Rawat, S., Goel, N., Shelkar, S., Kumar, V., 2020. Radiation grafted cellulose fabric as reusable anionic adsorbent: A novel strategy for potential large-scale dye wastewater remediation. Carbohydr. Polymers 249, 116902. http://dx.doi.org/10.1016/j.carbpol.2020.116902.
Mohammed, J.T., Azeez, A.R., Lutffe, T., 2015. Biosorption of copper from synthesized wastewater using agriculture waste (Roasted date pits). Int. J. Recent Sci. Res. 6 (3), 3063–3068.
Mvulirwenande, S., Wehn, U., 2020. Dynamics of water innovation in african cities: Insights from Kenya, Ghana and Mozambique. Environ. Sci. Policy 114, 96–108. http://dx.doi.org/10.1016/j.envsci.2020.07.024.
Naeimi, S., Faghihian, H., 2017. Performance of novel adsorbent prepared by magnetic metal-organic framework (MOF) modified by potassium nickel hexacyanoferrate for removal of Cs + from aqueous solution. Separation And Purification Technology 175, 255–265. http://dx.doi.org/10.1016/j.seppur.2016.11.028.
Naidu, G., Loganathan, P., Jeong, S., Johir, M., To, V., Kandasamy, J., Vigneswaran, S., 2016. Rubidium extraction using an organic polymer encapsulated potassium copper hexacyanoferrate sorbent. Chem. Eng. J. 306, 31–42.
Nandiyanto, A., Santiuly Girsang, G., Maryanti, R., Ragadhita, R., Anggraeni, S., Fauzi, F., et al., 2020. Isotherm adsorption characteristics of carbon microparticles prepared from pineapple peel waste. Commun. Sci. Technol. 5 (1), 31–39. http://dx.doi.org/10.21924/cst.5.1.2020.176.
Nassrullah, H., Anis, S., Hashaikeh, R., Hilal, N., 2020. Energy for desalination: A state-of-the-art review. Desalination 491, 114569. http://dx.doi.org/10.1016/j.desal.2020.114569.
Núñez-Gómez, D., Rodrigues, C., Lapolli, F., Lobo-Recio, M., 2019. Adsorption of heavy metals from coal acid mine drainage by shrimp shell waste: Isotherm and continuous-flow studies. J. Environ. Chem. Eng. 7 (1), 102787. http://dx.doi.org/10.1016/j.jece.2018.11.032.
Nur, T., Loganathan, P., Johir, M., Kandasamy, J., Vigneswaran, S., 2018. Removing rubidium using potassium cobalt hexacyanoferrate in the membrane adsorption hybrid system. Separation And Purification Technology 191, 286–294. http://dx.doi.org/10.1016/j.seppur.2017.09.048.
Oliveira, P., Kalinke, C., Mangrich, A., Marcolino-Junior, L., Bergamini, M., 2018. Copper hexacyanoferrate nanoparticles supported on biochar for amperometric determination of isoniazid. Electrochim. Acta 285, 373–380. http://dx.doi.org/10.1016/j.electacta.2018.08.004.
Pelalak, R., Heidari, Z., Khatami, S., Kurniawan, T., Marjani, A., Shirazian, S., 2021. Oak wood ash/GO/Fe3O4 adsorption efficiencies for cadmium and lead removal from aqueous solution: Kinetics, equilibrium and thermodynamic evaluation. Arab. J. Chem. 14 (3), 102991. http://dx.doi.org/10.1016/j.arabjc.2021.102991.
Rahman, H., Zaidi, S.J., 2018. Desalination in Qatar: Present status and future prospects. Civil Eng. Res. J. 6 (5), http://dx.doi.org/10.19080/cerj.2018.06.555700.
Rizzi, V., D'Agostino, F., Fini, P., Semeraro, P., Cosma, P., 2017. An interesting environmental friendly cleanup: The excellent potential of olive pomace for disperse blue adsorption/desorption from wastewater. J. Dyes Pigments 140, 480–490.
Ryu, J., Hong, J., Park, I., Ryu, T., Hong, 2020. Recovery of strontium (Sr2+) from seawater using a hierarchically structured MnO2/C/Fe3O4 magnetic nanocomposite. Hydrometallurgy 191, 105224. http://dx.doi.org/10.1016/j.hydromet.2019.105224.
Saad, E., Mansour, R., El-Asmy, A., El-Shahawi, M., 2008. Sorption profile and chromatographic separation of uranium (VI) ions from aqueous solutions onto date pits solid sorbent. Talanta 76 (5), 1041–1046. http://dx.doi.org/10.1016/j.talanta.2008.04.065.
Shadman, S., Daneshi, M., Shafiei, F., Azimimehr, M., Khorasgani, M., Sadeghian, M., et al., 2019. Aptamer-based electrochemical biosensors. Electrochem. Biosensors 213–251. http://dx.doi.org/10.1016/b978-0-12-816491-4.00008-5.
Snyders, C., Bradshaw, S., Akdogan, G., Eksteen, J., 2014. The effect of temperature cyanide and base metals on the adsorption of Pt, Pd and Au onto activated carbon. Hydrometallurgy 149, 132–142.
Tang, L., Gou, S., He, Y., Liu, L., Fang, S., Duan, W., Liu, T., 2021. An efficient chitosan-based adsorption material containing phosphoric acid and amidoxime groups for the enrichment of Cu (II) and Ni (II) from water. J. Molecular Liquids 115815. http://dx.doi.org/10.1016/j.molliq.2021.115815.
Thanarasu, A., Periyasamy, K., Periyaraman, P., Devaraj, T., Velayutham, K., Subramanian, S., 2019. Comparative studies on adsorption of dye and heavy metal ions from effluents using eco-friendly adsorbent. Materials Today: Proceedings http://dx.doi.org/10.1016/j.matpr.2020.07.001.
Tian, L., Ma, W., Han, M., 2010. Adsorption behavior of Li+ onto nano-lithium ion sieve from hybrid magnesium/lithium manganese oxide. Chem. Eng. J. 156 (1), 134–140. http://dx.doi.org/10.1016/j.cej.2009.10.008.
Vadi, M., Mansoorabad, A., Mohammadi, M., Rostami, N., 2013. Investigation of langmuir, freundlich and temkin adsorption isotherm of tramadol by multi-wall carbon nanotube. Asian J. Chem. 25 (10), 5467–5469. http://dx.doi.org/10.14233/ajchem.2013.14786.
Wadhawan, S., Jain, A., Nayyar, J., Mehta, S., 2020. Role of nanomaterials as adsorbents in heavy metal ion removal from waste water: A review. J. Water Process Eng. 33, 101038. http://dx.doi.org/10.1016/j.jwpe.2019.101038.
Wahib, S., Da'na, D., Zaouri, N., Hijji, Y., Al-Ghouti, M., 2021. Adsorption and recovery of lithium ions from groundwater using date pits impregnated with cellulose nanocrystals and ionic liquid. J. Hard Mater. 421, 126657. http://dx.doi.org/10.1016/j.jhazmat.2021.126657.
Wan, L., Wang, H., 2021. Control of urban river water pollution is studied based on SMS. Environ. Technol. Innov. 22, 101468. http://dx.doi.org/10.1016/j.eti.2021.101468.
Wang, H., Luo, W., Tian, Z., Ouyang, C., 2019. First principles study of alkali and alkaline earth metal ions adsorption and diffusion on penta-graphene. Solid State Ionics 342, 115062. http://dx.doi.org/10.1016/j.ssi.2019.115062.
Wang, J., Zhuang, S., Liu, Y., 2018. Metal hexacyanoferrates-based adsorbents for cesium removal. Coord. Chem. Rev. 374, 430–438. http://dx.doi.org/10.1016/j.ccr.2018.07.014.
Weber, T., Chakravorti, R., 1974. Pore and solid diffusion models for fixed-bed adsorbers. AIChE J. 20 (2), 228–238.
WHO, 1996. Guidelines for Drinking-Water Quality - Second Edition - Health Criteria and Other Supporting Information. Volume 2.
WHO, 2000. Chapter 6.12. Vanadium. Retrieved from https://www.euro.who.int/__data/assets/pdf_file/0016/123082/AQG2ndEd_6_12vana.
WHO, 2010. Strontium and Strontium Compounds. Retrieved from: https://www.who.int/ipcs/publications/cicad/cicad77.pdf.
WHO. 2011. Guidelines for Drinking-water Quality, 4th ed., Geneva, 229–230, 433–434.
Wiśniewska, M., Fijałkowska, G., Ostolska, I., Franus, W., Nosal-Wiercińska, A., Tomaszewska, B., et al., 2018. Investigations of the possibility of lithium acquisition from geothermal water using natural and synthetic zeolites applying poly(acrylic acid). J. Cleaner Prod. 195, 821–830. http://dx.doi.org/10.1016/j.jclepro.2018.05.287.
Xiao, J., Nie, X., Sun, S., Song, X., Li, P., Yu, J., 2015. Lithium ion adsorption–desorption properties on spinel Li4Mn5O12 and pH-dependent ion-exchange model. Adv. Powder Technol. 26 (2), 589–594. http://dx.doi.org/10.1016/j.apt.2015.01.008.
Yadav, S., Asthana, A., Singh, A., Chakraborty, R., Vidya, S., Susan, M., Carabineiro, S., 2021. Adsorption of cationic dyes, drugs and metal from aqueous solutions using a polymer composite of magnetic/β-cyclodextrin/activated charcoal/Na alginate: Isotherm, kinetics and regeneration studies. J. Hard Mater. 409, 124840. http://dx.doi.org/10.1016/j.jhazmat.2020.124840.
Yadav, M., Gupta, R., Sharma, R., 2019. Green and sustainable pathways for wastewater purification. In: Advances in Water Purification Techniques. pp. 355–383. http://dx.doi.org/10.1016/b978-0-12-814790-0.00014-4.

Yang, W., Wang, Z., Song, S., Han, J., Chen, H., Wang, X., 2019. Adsorption of copper(II) and lead(II) from seawater using hydrothermal biochar derived from Enteromorpha. Mar. Pollut. Bull. 149, 110586. http://dx.doi.org/10.1016/j.marpolbul.2019.110586.

Yu, H., Zi, F., Hu, X., Nie, Y., Chen, Y., Cheng, H., 2017. Adsorption of gold from thiosulfate solutions with chemically modified activated carbon. Adsorption Science & Technology 36 (1-2), 408–428. http://dx.doi.org/10.1177/0263617417698864.

Yuan, C., Zhang, L., Li, H., 2019. Highly selective lithium ion adsorbents: Polymeric porous microsphere with crown ether groups. Trans. Tianjin Univ. 25, 101–109. http://dx.doi.org/10.1007/s12209-018-0147-5.

Zeldowitsch, J., 1934. Adsorption site energy distribution. Acta Phys.-Chim. 961–973.

Zhang, B., Chen, Y., 2020. Particle size effect on pore structure characteristics of lignite determined via low-temperature nitrogen adsorption. J. Nat. Gas Sci. Eng. 84, 103633. http://dx.doi.org/10.1016/j.jngse.2020.103633.

Zhang, Q., Li, S., Sun, S., Yin, X., Yu, J., 2010. Limn2o4 spinel direct synthesis and lithium ion selective adsorption. Chem. Eng. Sci. 65 (1), 169–173. http://dx.doi.org/10.1016/j.ces.2009.06.045.

Zhang, X., Liu, Y., 2020. Ultrafast removal of radioactive strontium ions from contaminated water by nanostructured layered sodium vanadosilicate with high adsorption capacity and selectivity. J. Hazardous Mater. 398, 122907. http://dx.doi.org/10.1016/j.jhazmat.2020.122907.

Zhong, J., Lin, S., Yu, J., 2021. Lithium recovery from ultrahigh Mg2+/Li+ ratio brine using a novel granulated Li/Al-LDHs adsorbent. Separation And Purification Technology 256, 117780. http://dx.doi.org/10.1016/j.seppur.2020.117780.

Zhou, X., Liu, D., Bu, H., Deng, L., Liu, H., Yuan, P., et al., 2017. XRD-based quantitative analysis of clay minerals using reference intensity ratios mineral intensity factors, Rietveld, and full pattern summation methods: A critical review. Solid Earth Sciences 3 (1), 16–29. http://dx.doi.org/10.1016/j.sesci.2017.12.002.

Zhuang, S., Wang, J., 2019. Removal of cesium ions using nickel hexacyanoferrates-loaded bacterial cellulose membrane as an effective adsorbent. J. Molecular Liquids 294, 111682. http://dx.doi.org/10.1016/j.molliq.2019.111682.